



Significance of Climate Indices to Benthic Conditions Across the Northern North Atlantic and Adjacent Shelf Seas

Clare Johnson*, Mark Inall, Stefan Gary and Stuart Cunningham

Scottish Association for Marine Science, Oban, United Kingdom

OPEN ACCESS

Edited by:

J. Murray Roberts,
University of Edinburgh,
United Kingdom

Reviewed by:

Michael Vecchione,
National Oceanic and Atmospheric
Administration (NOAA), United States
Martin George White,
National University of Ireland Galway,
Ireland

*Correspondence:

Clare Johnson
clare.johnson@sams.ac.uk;
cljo@sams.ac.uk

Specialty section:

This article was submitted to
Deep-Sea Environments and Ecology,
a section of the journal
Frontiers in Marine Science

Received: 28 March 2019

Accepted: 07 January 2020

Published: 23 January 2020

Citation:

Johnson C, Inall M, Gary S and
Cunningham S (2020) Significance
of Climate Indices to Benthic
Conditions Across the Northern North
Atlantic and Adjacent Shelf Seas.
Front. Mar. Sci. 7:2.
doi: 10.3389/fmars.2020.00002

The northern North Atlantic Ocean and its adjacent shelf seas, are influenced by several large-scale physical processes which can be described by various climate indices. Although the signal of these indices on the upper ocean has been investigated, the potential effects on vulnerable benthic ecosystems remains unknown. In this study, we examine the relationship between pertinent climate indices and bottom conditions across the northern North Atlantic region for the first time. Changes are assessed using a composite approach over a 50 year period. We use an objectively-analyzed observational dataset to investigate changes in bottom salinity and potential temperature, and output from a high-resolution ocean model to examine changes in bottom kinetic energy. Statistically significant, and spatially coherent, changes in bottom potential temperature and salinity are seen for the North Atlantic Oscillation (NAO), Atlantic Meridional Overturning Circulation (AMOC), Atlantic Multi-decadal Oscillation (AMO), and Subpolar Gyre (SPG); with statistically significant changes in bottom kinetic energy seen in the subpolar boundary currents for the NAO and AMOC. As the climate indices have multi-annual timescales, changes in bottom conditions may persist for several years exposing sessile benthic ecosystems to sustained changes. Variations in baseline conditions will also alter the likelihood of extreme events such as marine heatwaves, and will modify any longer-term trends. A thorough understanding of natural variability and its effect on benthic conditions is thus essential for the evaluation of future scenarios and management frameworks.

Keywords: benthic temperature, benthic salinity, benthic kinetic energy, Atlantic Meridional Overturning Circulation (AMOC), North Atlantic Oscillation (NAO), Atlantic Multi-decadal Oscillation (AMO), Subpolar Gyre Index

INTRODUCTION

The northern North Atlantic region contains a number of deep-sea ecosystems including cold water corals, sponges, and those in hydrothermal fields, with some being classified as Vulnerable Marine Ecosystems (VMEs). These ecosystems are susceptible to changes in climate (Sweetman et al., 2017; Johnson et al., 2018), however, in order to place future changes in

context and evaluate management measures, it is vital to understand natural climate variability. Whilst the signals of various climate indices on upper ocean conditions have been investigated (e.g., Hátún et al., 2005; Frajka-Williams et al., 2017), potential effects on benthic conditions, and deep-sea VMEs, remain unknown. In this paper, we ask whether climate indices are associated with statistically significant, and spatially coherent, changes in bottom conditions across the northern North Atlantic region. To achieve this, we use an objectively-analyzed observational dataset (EN4) to investigate changes in bottom salinity and potential temperature, and output from a high-resolution ocean model (Viking20) to examine changes in bottom kinetic energy. We provide a first look at the emergent patterns, and examine and describe their spatial coherency and magnitudes. We make some tentative explanations for the physical basis of some of the significant signals, but are careful not to ascribe causality where we investigate only correlation.

CLIMATE INDICES

The northern North Atlantic region, which we here define as that north of 30° N including its adjoining continental shelves and seas (**Figure 1**), has several multi-annual large-scale physical processes that influence upper ocean climate and have the potential to effect deep-sea ecosystems. These processes are often described using a number of basin-scale climate “indices”; the most common being the: North Atlantic Oscillation (NAO), the strength of the Atlantic Meridional Overturning Circulation (AMOC), the Atlantic Multi-decadal Oscillation (AMO), and the strength and extent of the Subpolar Gyre (SPG). Time-series of these indices are shown in **Figure 2**. It should be noted that although we consider each climate index individually, it is likely that they are not fully independent of one another. For example, the SPG may alter ocean heat content and therefore influence the AMO (Häkkinen et al., 2013). Similarly, atmospheric pressure changes related to the NAO may affect the AMO through changes in upper water properties (Yashayaev and Seidov, 2015) and the SPG (Häkkinen et al., 2011). Additionally, model studies suggest a possible link between the AMO and the AMOC on longer time-scales (Zhang, 2008; Buckley and Marshall, 2016), although no relationship has been established in the observational record (Lozier, 2010). Despite these possible inter-dependencies, we follow many previous studies (e.g., Hurrell, 1995; Häkkinen et al., 2011; Tulloch and Marshall, 2012; Yeager, 2015) and consider an index individually. This enables us to interpret our results in the context of other research, and investigate if any indices produce similar patterns of variability.

North Atlantic Oscillation (NAO)

The NAO is an atmospheric pressure index that influences the position and strength of westerly winds (e.g., Hurrell, 1995) and has several effects on the North Atlantic ocean. Sea surface temperatures show a tripole pattern; during a positive NAO: cooler temperatures are seen south of our study area in the tropical Atlantic, warmer temperatures are observed in the Gulf Stream region in the western Atlantic south of ~45°N, and cooler

temperatures are seen in the main subpolar region centered about Greenland (e.g., Marshall et al., 2001). A further area of warmer temperatures, during a positive NAO, is observed on the western European Shelf extending to the oceanic regions immediately west of the UK and Norway (Visbeck et al., 2013). The NAO also effects the intensity of convection in the Labrador and Nordic Seas, which, along with changes in upper waters, determines the properties of intermediate and deep water masses in those basins (Dickson et al., 1996). A positive NAO is associated with cooler and fresher Labrador Sea Water (e.g., Yashayaev, 2007). This signature is spread through the subpolar gyre along the Labrador Sea Water pathways, although transit times to the eastern basins are in the order of 5–10 years (Yashayaev et al., 2007a,b). In contrast, deep waters in the Greenland Sea are warmer and more saline during a high NAO (Dickson et al., 1996; Alekseev et al., 2001). Finally, Iceland Scotland Overflow Water has a lower salinity during a high NAO (Sarafanov, 2009) with less vigorous flow (Boessenkool et al., 2007). No relationship between Denmark Strait Overflow Water salinities and the NAO is observed (Sarafanov, 2009).

Atlantic Meridional Overturning Circulation (AMOC)

The AMOC is a measure of the strength of the overturning circulation in the important North Atlantic region. This circulation involves the conversion of less dense upper waters to denser intermediate and deep waters, and comprises a northward flow in the upper water column balanced by a return flow at depth. The patterns in upper ocean properties have predominantly been investigated in models, with temperatures showing a dipole signal: during a strong AMOC, cooler temperatures are observed in the Gulf Stream region, and warmer temperatures in the subpolar North Atlantic (Zhang, 2008; Tulloch and Marshall, 2012). In observational datasets, warmer sea surface temperatures in the Gulf Stream region, and cooler sea surface temperatures in the subpolar North Atlantic, have been attributed to a weakening AMOC over the past century (e.g., Caesar et al., 2018). This cooling is most pronounced in the Labrador, Irminger and Iceland Basins.

Atlantic Multi-decadal Oscillation (AMO)

The AMO is a measure of mean sea surface temperature over the entire North Atlantic and exhibits low frequency variability with a periodicity in the order of 65–80 years (Kerr, 2000). A positive index is associated with warmer sea surface temperatures over the region, with the greatest warming observed in the western subpolar gyre (Buckley and Marshall, 2016). During negative phases of the AMO, zonally-averaged sea surface temperature anomalies reveal the cooling is also more pronounced north of around 40° N (Frajka-Williams et al., 2017).

Subpolar Gyre (SPG)

The SPG is a measure of both the strength and extent of the subpolar gyre, with the most commonly used index being the first principal component of the sea surface height field (e.g.,

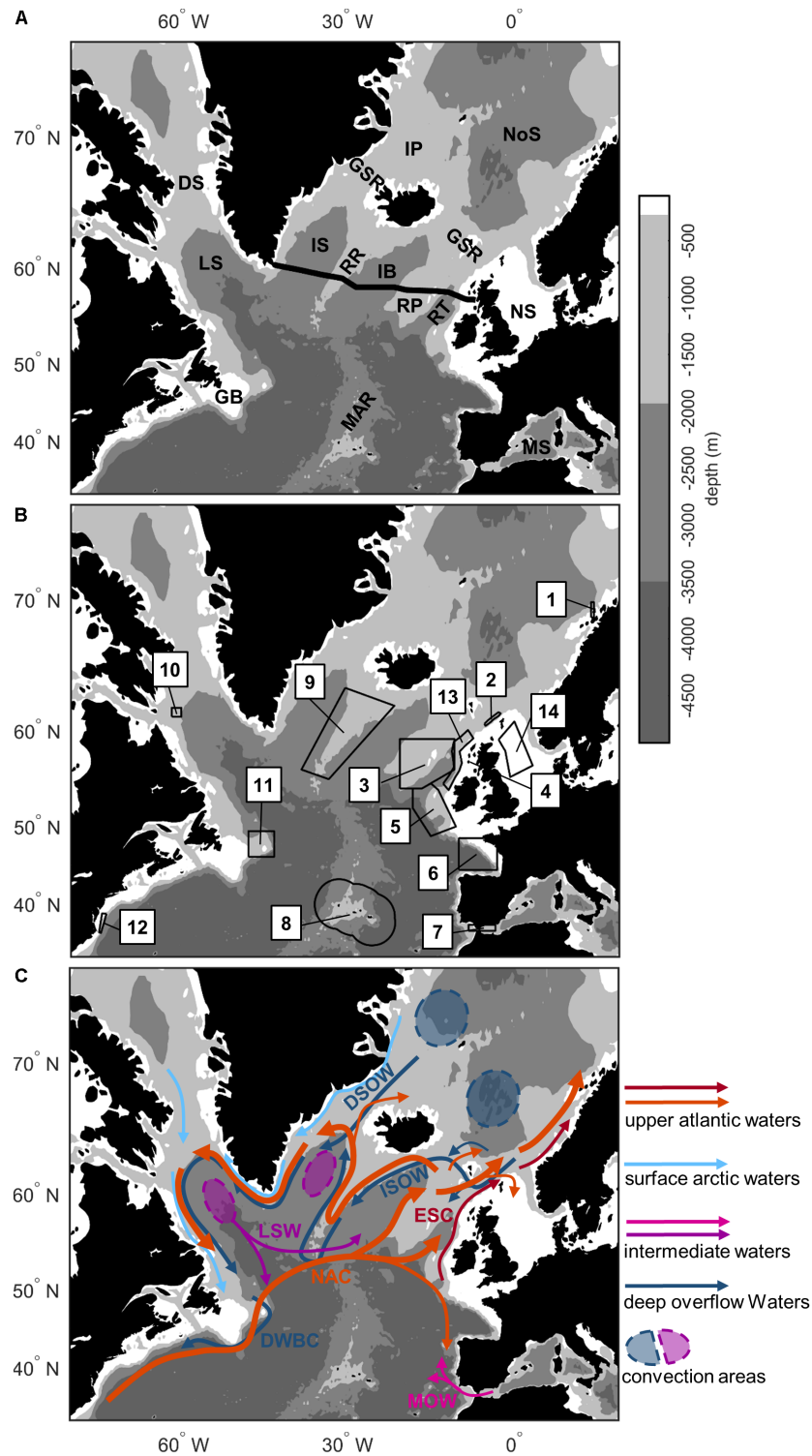
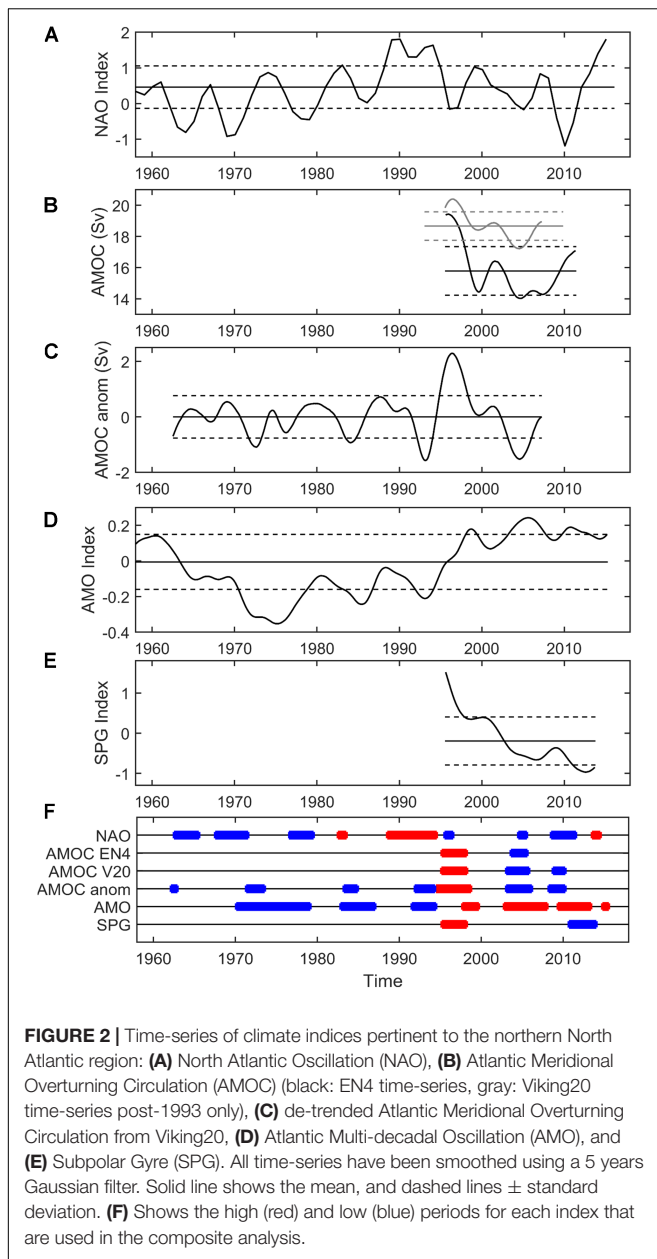


FIGURE 1 | Map of the northern North Atlantic region showing (A) bathymetric features referred to in the text, (B) the 14 case studies chosen to represent a range of Atlantic Vulnerable Marine Ecosystems and management regimes, and (C) a schematic of the circulation. See **Table 1** for case study names. Black line in (A) shows the OSNAP-EAST section. Labeled bathymetry: DS, Davis Strait; GB, Grand Banks region; GSR, Greenland-Scotland Ridge; IB, Iceland Basin; IP, Icelandic Plateau; IS, Irminger Sea; LS, Labrador Sea; MAR, Mid-Atlantic Ridge; MS, Mediterranean Sea; NS, North Sea; NoS, Nordic Seas; RR, Reykjanes Ridge; RP, Rockall-Hatton Plateau; RT, Rockall Trough. Contour levels are at 200, 2000, and 3500 m denoting the continental shelves, maximum depth of ARGO floats, and abyssal areas. Labeled currents, DSOW, Denmark Strait Overflow Water; DWBC, Deep Western Boundary Current; ESC, European Slope Current; ISOW, Iceland Scotland Overflow Waters; LSW, Labrador Sea Water; MOW, Mediterranean Overflow Water; NAC, North Atlantic Current.



Häkkinen and Rhines, 2004; Hátún et al., 2005). During a high SPG, the subpolar gyre is stronger and expands eastward (Thierry et al., 2008). Eastern areas of the subpolar North Atlantic are more strongly influenced by cooler and fresher subpolar water masses, with a reduction in the presence of warmer and saltier subtropical and inter-gyre water masses that enter from the southeast. This change is reflected in upper water properties, with lower temperatures and salinities observed in eastern areas during a high SPG (Holliday, 2003; Johnson et al., 2013). Similarly, at intermediate depths, cooler and fresher conditions are also seen during a high SPG due to the increased influence of Labrador Sea Water and reduced influence of warmer and saltier Mediterranean Water (Lozier and Stewart, 2008).

DATA AND METHODS

In this work, we use an objectively-analyzed observational dataset (EN4) to examine changes in bottom salinity (S_{bot}) and potential temperature (θ_{bot}), and output from a high-resolution, eddy-resolving ocean-only model (Viking20) to investigate changes in bottom kinetic energy (KE_{bot}).

EN4 Data

EN4 is a global, quality-controlled, objectively-analyzed, dataset of observed potential temperature and salinity profiles which has been used extensively (e.g., Prieto et al., 2015; Yang et al., 2016; Zunino et al., 2017; Chafik et al., 2019; Etourneau et al., 2019). It combines data from all types of profiling instruments, including ship-based measurements and ARGO floats, and is available as monthly averages (Good et al., 2013). EN4 has a 1° horizontal resolution meaning that smaller spatial features will not be resolved, and that large property gradients, such as around the boundary of basins, will become smoothed. Although EN4 starts in 1900, we limit our analysis to 1959 onward (to match with Viking20) but extend the analysis until December 2017 to maximize available data.

Bottom potential temperature and salinity were defined as values in the deepest depth bin at any location. The vertical grid in EN4 varies non-linearly with water depth, ranging from 10 m bins in the upper 100 m, to a maximum of ~ 300 m below 3000 m. Thus measurements at any location will, at the most, be within 300 m of the sea-bed, with this value reducing as the sea-bed shallows. This vertical resolution is unlikely to greatly impact the representativeness of bottom values when the deep waters are weakly stratified; however, any vertical features smaller than the grid box depth will not be resolved. The EN4 dataset reverts to a 1971–2000 climatology in the absence of any observations (Good et al., 2013). Information for each data point (i.e., for each horizontal grid point, and at each depth level) is given in the weighting variable, which ranges from approximately zero to one. A value of zero indicates the absence of any observations for that data point, during that month, and that climatology is used. Conversely, a weighting of approximately one indicates a high influence of observations. Here we use a cut-off weighting value of 0.1, i.e., we do not use data with a weighting < 0.1 . This value was chosen to ensure that periods with no observations, where EN4 reverts to a pure climatology, were not included in the analyses, whilst as many observations as possible were incorporated.

Viking20 Data

Viking20 is a $1/20$ th degree, hindcast-forced, ocean-only model, covering the northern North Atlantic area. It is nested within a global ocean/sea-ice model using the Adaptive Grid Refinement Scheme (Debreu et al., 2008). The model was initiated with climatological temperature and salinity values, and was forced with CORE2 atmospheric data (Large and Yeager, 2009). More details of the model configuration can be found in Böning et al. (2016). Viking20 has been used in many studies, including those to investigate: the North Atlantic Current (Breckenfelder et al., 2017), convection in the Labrador Sea (Böning et al., 2016),

Denmark Strait Overflow Water (Behrens et al., 2017), the Deep Western Boundary Current (Mertens et al., 2014; Handmann et al., 2018), and seasonal changes in the eastern subpolar North Atlantic (Gary et al., 2018).

We use Viking20 output as 5 days averages from 1959 to 2009 to investigate changes in bottom kinetic energy. Bottom horizontal velocities (u_{bot} , v_{bot}) were extracted from the bottom grid point at a particular location. As for EN4, grid box thickness varies non-linearly with depth; from <10 m in the upper 50 m, to a maximum of ~250 m in the deepest points of the model domain. The vertical resolution of Viking20 is not dissimilar to that of EN4, and the same limitations apply. For example, real-world smaller-scale frictional effects, such as benthic boundary layers, will not be resolved in the velocity field. As our goal was to study kinetic energy, rather than velocities, u_{bot} and v_{bot} were first linearly interpolated from their respective grids onto the grid containing θ_{bot} and S_{bot} . Bottom mean kinetic energy was then calculated as the sum of the squares of mean u_{bot} and v_{bot} , with the eddy kinetic energy defined as the sum of the variances of u_{bot} and v_{bot} . As our data are 5 days averages, variances represent energy of sub-inertial flows.

Ecosystem Case Studies

As well as considering spatio-temporal patterns at the basin-scale, we examine temporal changes at fourteen case study sites (Figure 1 and Table 1). These sites were chosen to represent a variety of potentially vulnerable deep-sea ecosystems across the northern North Atlantic region as indicated by VME indicator records (Morato et al., 2018). The sites also include a number of existing, or proposed, Marine Protected Areas (MPAs), Ecologically or Biologically Significant Areas (EBSAs), and VME closures (Johnson et al., 2018). Although

four sites have maximum depths below 3500 m (Table 1), there is no site that truly represents the abyssal plains of the North Atlantic south of 50°N. This reflects the current absence of VME indicator records in these areas (Morato et al., 2018). Time-series were constructed for each case study site. In EN4, data within each case study polygon were simply averaged for each monthly time-step. As case studies 4 and 10 did not contain any EN4 grid points; time-series for these sites were instead extracted from the nearest EN4 grid point. In Viking20, the model grid is curvilinear. Thus, grid points were accordingly area weighted when calculating averages for each 5 days time-step.

Climate Indices

We consider the four most commonly used climate indices for the North Atlantic Ocean: the NAO, AMOC, AMO, and SPG. The NAO index used is defined as the normalized pressure difference between Gibraltar and southwest Iceland (Jones et al., 1997). Data were downloaded from the Climatic Research Unit¹ and the winter (DJFM) mean calculated. As Viking20 is forced with CORE2 atmospheric data, which will include a signature of the NAO, we use the observational NAO time-series to investigate ocean correlations in both the EN4 and Viking20 datasets.

For the AMOC, we use the commonly used definition of the maximum in the overturning stream function in density space (e.g., Mercier et al., 2015; Lozier et al., 2019). As this index is calculated from oceanic rather than atmospheric variables, and changes in the model and observational AMOC may not be contemporaneous, we compute two AMOC time-series: one from EN4 and one from Viking20. For the observational dataset we used the method of Mercier et al. (2015), but using EN4 data along the OSNAP-EAST section (black line, Figure 1A). Geostrophic velocities perpendicular to the section were calculated from EN4 temperature and salinity data and referenced to satellite altimetry data. The Viking20 AMOC time-series was calculated using model velocities perpendicular to the OSNAP-EAST section.

We use an AMO index downloaded from the National Oceanic and Atmospheric Administration² as monthly averages. This time-series consists of sea surface temperatures, averaged over 0–70°N before de-trending using a 10 year running mean (Enfield et al., 2001). The AMO is also an oceanic index, suggesting that again a model and observational time-series is required. Although the construction of an AMO index from Viking20 was considered, it was discounted for two reasons. Firstly, the AMO index is calculated using sea surface temperatures over the entire North Atlantic; however, the Viking20 nested model domain starts at 32° N (Böning et al., 2016). This makes the calculation of an AMO index from Viking20 more complex. Secondly, Viking20 is an ocean-only model meaning that feedbacks between the ocean and atmosphere are not fully represented. As previous work suggests there is a requirement for fully-coupled models in order to represent important teleconnections

TABLE 1 | Description of case study regions chosen to represent a range of Atlantic Vulnerable Marine Ecosystems and management regimes.

Case studies	Area ($\times 10^3$ km ²)	Mean depth (m)	Std depth (m)	Min. depth (m)	Max. depth (m)
1 LoVe Observatory	2.2	746	806	1	2298
2 Western Scottish Slope	5.3	596	133	234	952
3 Rockall Bank	301.4	1470	746	21	3026
4 Mingulay Reef	0.1	196	25	148	230
5 Porcupine Sea Bight	218.2	2187	1517	39	4844
6 Bay of Biscay	238.5	2744	2073	1	5026
7 Gulf of Cadiz/Alboran Sea	43.4	697	434	1	1872
8 Azores	954.2	3064	1104	1	5627
9 Reykjanes Ridge	388.1	1927	453	499	3209
10 Davis Strait	8.2	962	537	518	2319
11 Flemish Cap	124.4	1471	1218	128	4664
12 USA Mid-Atlantic Canyons	16.5	750	717	32	2205
13 European Slope	61.2	1243	807	57	3009
14 North Sea	112.0	99	25	40	179

All statistics exclude areas of land and were calculated using ETOPO2 bathymetry.

¹<https://crudata.uea.ac.uk/cru/data/nao/>

²<https://www.esrl.noaa.gov/psd/data/timeseries/AMO/>

(Ruprich-Robert et al., 2017), we focus on the observational AMO index and therefore do not investigate changes in KE_{bot} using Viking20.

The SPG index used is defined as the first principal component of the sea surface height field between 40 and 65° N and 60° W to 10° E (Berx and Payne, 2017). This was downloaded from <https://data.marine.gov.scot/dataset/sub-polar-gyre-index> as monthly averages. Again, we considered extracting out a model-based SPG time-series from Viking20 to use in conjunction with the observational index. However, the basin-averaged sea surface height field in Viking20 exhibits a drift after the mid-1990s, which would redistribute power among the principal components used to generate the SPG index. As such, we again focus on the observational SPG and interrogate only the EN4 dataset. Although there may be a large-scale drift in the Viking20 sea surface height field, gradients in sea surface height and the overall circulation patterns in the model output compare well to observations (e.g., Breckenfelder et al., 2017; Gary et al., 2018).

Composite Method

In order to investigate any differences in near-bed conditions associated with each climate index, we use the commonly-used composite method (e.g., Terray et al., 2003; Häkkinen et al., 2011; Tulloch and Marshall, 2012). For each climate index, “high years” were defined as those exceeding one standard deviation above the mean, and “low years” as those less than one standard deviation below the mean. Composites for the high and low climate states were calculated by averaging properties from all high and low years respectively. One of the limitations of the composite approach is that it only considers high and low states, and not transitional processes between the two. As the Viking20 AMOC time-series shows a long-term trend and we are interested in multi-annual changes, we de-trended this index before creating the composites. The time-series was de-trended by assuming a linear long-term trend which may not be entirely appropriate for low-frequency oscillations. However, the record is too short to establish any low-frequency variability more accurately, and de-trending enables us to investigate multi-annual changes over a 50 year period. The number of months averaged to create each composite are shown in **Table 2**.

The statistical significance of observed changes at the 95% confidence level were tested using the method detailed in

Terray et al. (2003), which we briefly describe here. At each grid point (X), we assess whether the values observed during the high years, or the low years (class j), are significantly different from a combined group made up of high and low years only. The years within one standard deviation from the mean are not included because the composite analysis only compares two groups: high and low years. The mean of class j (\bar{x}_j) is therefore compared to the mean of the combined high and low time-series (\bar{x}), with respect to the standard error (Equations 1, 2).

$$U(X) = \text{abs}((\bar{x}_j - \bar{x})/s_j) \quad (1)$$

$$s_j = \sqrt{(n - n_j)/(n_j \times (n - 1))} \times s \quad (2)$$

where: s is the standard deviation of the combined high and low time-series; and n and n_j the number of data points in the combined time-series and class j respectively.

This procedure tests whether or not the high and low years were allocated randomly from the combined group. If the high years and low years are allocated randomly, $U(X)$ will approach zero. Hence, the larger $U(X)$, the more diverse the high and low years, and the less likely that the high and low years were randomly selected. It should be noted that $U(X)$ calculated with the high years as class j , is identical to $U(X)$ calculated with the low years as class j . We set the critical value as 1.96, with values of $U(X)$ exceeding this indicating that the two means are statistically significantly different at the 95% confidence level.

RESULTS: LONG-TERM MEAN STATE

In order to provide a baseline for interpreting temporal changes, we first present the long-term mean and associated variability as basin-wide maps. Since the variability of shallower waters can be orders of magnitude larger than that of deeper waters, the variability maps are shown on a \log_{10} scale to highlight the changes over the whole domain. We use the objectively-analyzed observational dataset (EN4) to investigate changes in S_{bot} and θ_{bot} (**Figure 3**), and output from a high-resolution model (Viking20) to examine changes in KE_{bot} (**Figure 4**).

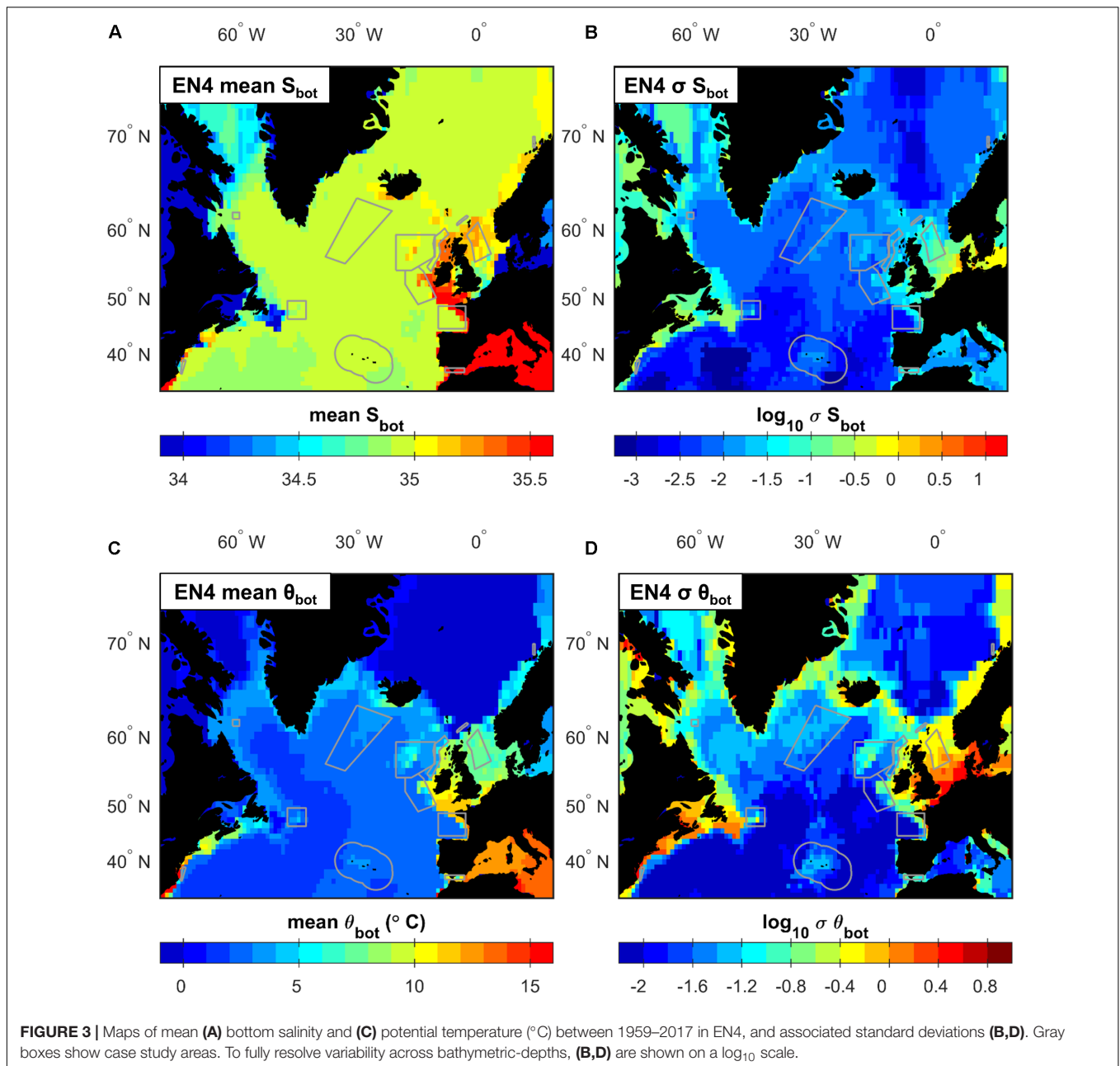
The lowest mean S_{bot} values are seen on the North American Shelf (<34.0) and in the Baltic Sea (<10.0), whilst the highest S_{bot} values are seen in the Mediterranean Sea (>37.0) and on the European Shelf west of the UK and Ireland (35.40–35.55) (**Figure 3A**). Relatively high S_{bot} values are also seen over the shallower Rockall-Hatton Plateau (35.0–35.3), over the eastern Greenland-Scotland Ridge (35.0–35.2), and along the Norwegian Coast (35.0–35.2). In contrast, fresher conditions (34.4–34.7) are seen north of the Davis Strait. Bottom salinity in areas deeper than ~2000 m is fairly uniform (34.85–35.00), although S_{bot} decreases with water depth, and slightly more saline bottom conditions are observed in eastern parts of the subpolar region. There is little difference between S_{bot} values in the northern North Atlantic and Nordic Seas.

Variability in S_{bot} is strongly related to water depth (**Figure 3B**), with the highest variability on the continental shelves (± 0.1 – 0.4), and the lowest variability seen in areas deeper

TABLE 2 | Number of months used to create the high and low composites for each climate index: North Atlantic Oscillation (NAO), Atlantic Meridional Overturning Circulation (AMOC), Atlantic Multi-decadal Oscillation (AMO), and Subpolar Gyre (SPG).

Climate index	Relevant figure	N_{high} (months)	N_{low} (months)
NAO	Figures 5, 6A	32	60
AMOC (EN4)	Figures 7A,B	28	16
AMOC (V20)	Figures 6B, 7C,D	43	98
AMO	Figure 8	112	169
SPG	Figure 9	28	32

For the AMOC two different time-series are used: (1) the EN4 time-series (black, **Figure 2B**), and (2) the 1959–2009 de-trended Viking20 time-series (**Figure 2C**).



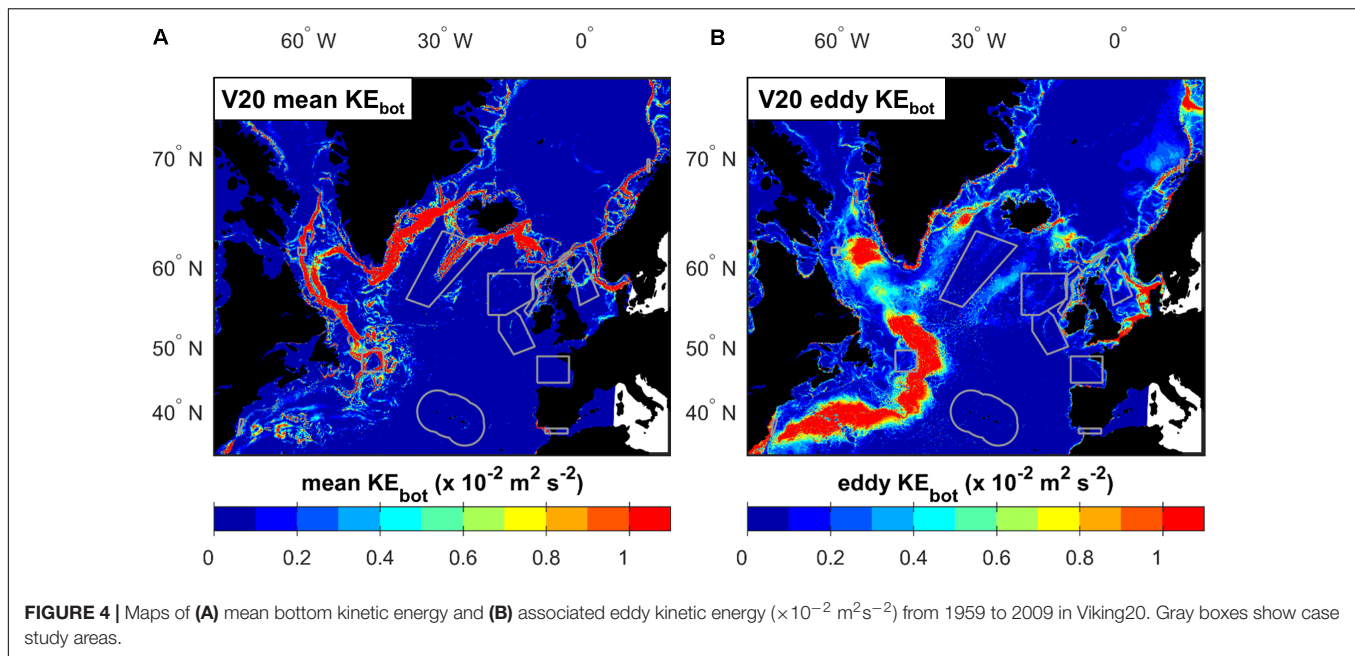
than 2000 m ($\pm < 0.01$). However, there is also spatial variability within these general descriptions. For example, variability is higher in the southern North Sea compared to the northern North Sea and shelf areas west of the UK and Ireland.

The highest θ_{bot} values ($> 15^{\circ}\text{C}$) are seen on the North American Shelf south of around 40°N and in the Mediterranean Sea ($> 12^{\circ}\text{C}$) (**Figure 3C**). Relatively high values are also seen in the southern North Sea and on the European Shelf west of the UK and Ireland (10 – 12°C). The coldest bottom conditions ($< 0^{\circ}\text{C}$) are seen in the Nordic Seas and north of the Davis Strait. In contrast, θ_{bot} values in the northern North Atlantic range from 1 to 3°C with an east-west split. Warmer θ_{bot} values are seen in areas shallower than approximately 2000 m, such as over

the Greenland-Scotland Ridge (3 – 5°C), around the boundaries of the subpolar basins (3 – 5°C), and over the Rockall-Hatton Plateau (4 – 7°C).

Variability in θ_{bot} is again mainly constrained by water depth (**Figure 3D**), with the highest values observed in the southern North Sea (± 2.0 – 4.0°C) and on the North American Shelf (± 1.5 – 3.0°C). In contrast, lower variability is observed in the deep northern North Atlantic and Nordic Seas ($\pm < 0.04^{\circ}\text{C}$). In the subpolar North Atlantic, higher variability (0.04 – 0.06°C) is observed in the Labrador Sea and Irminger Sea compared to the more eastern basins.

The highest KE_{bot} ($> 10 \times 10^2 \text{ m}^2\text{s}^{-2}$) (**Figure 4A**) is associated with the flow of Denmark Strait Overflow Water in



the Irminger Sea, and Iceland Scotland Overflow Water in the Iceland Basin. In addition, high KE_{bot} values ($1\text{--}10 \times 10^{-2} \text{ m}^2 \text{ s}^{-2}$) are observed in the cyclonic boundary currents of the subpolar gyre, including around the boundary of the Labrador Sea and in the Deep Western Boundary Current. Energetic conditions ($>1 \times 10^{-2} \text{ m}^2 \text{ s}^{-2}$) are also associated with the European Slope Current along the northern European and Norwegian Shelves. Other areas, such as the deep northern North Atlantic and Nordic Seas, have low KE_{bot} ($<0.1 \times 10^{-2} \text{ m}^2 \text{ s}^{-2}$).

The highest values of eddy KE_{bot} ($1\text{--}2 \times 10^{-2} \text{ m}^2 \text{ s}^{-2}$) (Figure 4B) are associated with the Deep Western Boundary Current, although this is over a wider spatial area than the higher KE_{bot} signal. High eddy KE_{bot} values ($\sim 1 \times 10^{-2} \text{ m}^2 \text{ s}^{-2}$) are likewise associated with the overflow currents, as well as in the convection areas of the Labrador and Irminger Seas. High eddy KE_{bot} is also seen in the European Slope Current, although this is of lower magnitude than that seen for the deeper currents. Finally, areas of higher eddy KE_{bot} are seen on the continental shelves; including in the southern North Sea, on the North American Shelf south of around 40°N , and on both the East and West Greenland Shelves.

RESULTS: SPATIAL VARIABILITY LINKED TO CLIMATE INDICES

Having described the long-term mean and variability, we now examine changes associated with each climate index in turn using the composite approach detailed in section Composite Method. Again, we use the objectively-analyzed observational EN4 dataset to investigate changes in S_{bot} and θ_{bot} , and output from the Viking20 model to examine changes in KE_{bot} . For EN4, we only describe changes where a cut-off weighting is exceeded for both the high and low composites; this ensures the exclusion

of periods with no observations. Plots comparing the spatial footprint of different cut-off weightings, ranging from 0.05 to 0.25, are shown in **Supplementary Figures S1–S4**. For the NAO, the spatial distribution of data for cut-off values ranging from 0.1 to 0.25 is almost identical. For the AMOC, AMO, and SPG there are some small differences; for example: in the eastern Nordic Seas and around the Reykjanes Ridge for the AMOC, in the eastern Nordic Seas and Iceland Basin for the AMO, and in the eastern Nordic Seas for the SPG. However, all cut-off weightings retain data: on the continental shelves, around the boundaries of the basins of the subpolar North Atlantic, over the Reykjanes Ridge, over the Greenland-Scotland Ridge, over the Icelandic Plateau, and around the boundaries of the Nordic Seas. We chose a cut-off weighting of 0.1 to retain as many observations as possible, with only areas where this is exceeded for both the high and low composites included. Although there is a level of subjectivity when choosing the EN4 cut-off weighting, as an additional control we carried out statistical testing (as detailed in section Composite Method). Only changes between the high and low years that are statistically significant at the 95% confidence level are discussed. As pure climatology would have no significant correlations, we can be sure that any statistically significant patterns are due to the presence of data.

North Atlantic Oscillation (NAO)

The largest changes in S_{bot} and θ_{bot} associated with the NAO are observed on the continental shelf areas (Figure 5). The European and North American Shelves are anti-correlated: when the NAO is high, warmer and more saline bottom conditions are seen in the North Sea but cooler and fresher values are seen around Grand Banks. Whilst bottom conditions in the Grand Banks area are -0.5 to -1.3°C cooler, and -0.1 to -0.25 fresher, during a high NAO period relative to a low NAO period, the North Sea bottom

values are 1.0–1.3°C warmer and 0.2–1.2 saltier. The area to the west of Norway is also 0.03–0.5°C warmer during high NAO periods compared to low NAO periods, although a corresponding S_{bot} signal is absent.

When investigating signals away from the continental shelves, there is limited observational data, particularly below 2000 m. Nevertheless, some spatially coherent and statistically significant changes can be seen. In the Mediterranean Sea, warmer and saltier bottom conditions (0–0.3°C and 0–0.02) are observed during a high NAO. In contrast, lower S_{bot} and θ_{bot} values (<-0.02 and $<-0.2^\circ\text{C}$ respectively) are seen in the subpolar gyre, for example around the boundaries of the Labrador Sea and Irminger Sea, over the Reykjanes Ridge, and over the Rockall-Hatton Plateau. In particular, less saline bottom conditions (–0.02 to –0.04) are observed in eastern areas extending on to the shelf west of Scotland, and over the Greenland-Scotland Ridge along pathways of the North Atlantic Current and European Shelf Current.

Viking20 output can be used to evaluate changes in KE_{bot} (Figure 6A). During a high NAO, bottom currents are enhanced along the eastern boundary of the northern North Atlantic with higher KE_{bot} stretching along the European and Norwegian Shelf break, and into the North Sea. This is likely to indicate a stronger European Slope Current during a high NAO. Higher KE_{bot} is also observed along the Denmark Strait Overflow Water pathways around the western boundary of the Irminger Sea, although lower KE_{bot} values are seen around the northern and western boundaries of the Iceland Basin which is influenced by Iceland Scotland Overflow Water. Finally, lower KE_{bot} is seen on shelf areas to the north and west of the Labrador Sea.

Atlantic Meridional Overturning Circulation (AMOC)

To investigate changes associated with the AMOC, we start by using the post-1993 observational AMOC time-series to examine changes in the EN4 dataset (Figures 7A,B). The North American, European and Norwegian Shelves all have lower S_{bot} values (–0.1 to –0.5) during high AMOC states. While θ_{bot} values are also lower (–0.4 to –0.8°C) on northern parts of the North American Shelf and around Grand Banks during a high AMOC, south of around 50°N warmer (0.5–2.5°C) bottom conditions are seen. Additionally, on the European Shelf, statistically significant changes in θ_{bot} (–0.4 to –0.8°C) are only observed in the northern areas of the North Sea. The lower θ_{bot} values during a high AMOC on the Norwegian Shelf are also less pronounced than the observed freshening. Hence, on the continental shelves, changes in S_{bot} and θ_{bot} associated with the NAO are not simply correlated.

Moving now to oceanic areas, fresher and in particular cooler conditions are seen in most regions during a high AMOC. The largest changes (up to –0.35°C and –0.05) are seen around the boundaries of the Labrador Sea, Irminger Sea and Iceland Basin, as well as over the Greenland-Scotland Ridge. Although S_{bot} and θ_{bot} are lower during a high AMOC in the majority of areas,

warmer and more saline bottom conditions are also seen. For example, the Rockall Trough and eastern Iceland Basin are up to 0.011 more saline during a high AMOC. More saline conditions are also observed in the eastern Nordic Seas. In contrast, areas of warmer bottom conditions during a high AMOC are patchy. Despite the higher S_{bot} values in the Rockall Trough during a high AMOC, fresher (0 to –0.05) conditions are still observed over the shallower Rockall-Hatton Plateau and on the European Shelf west of the UK.

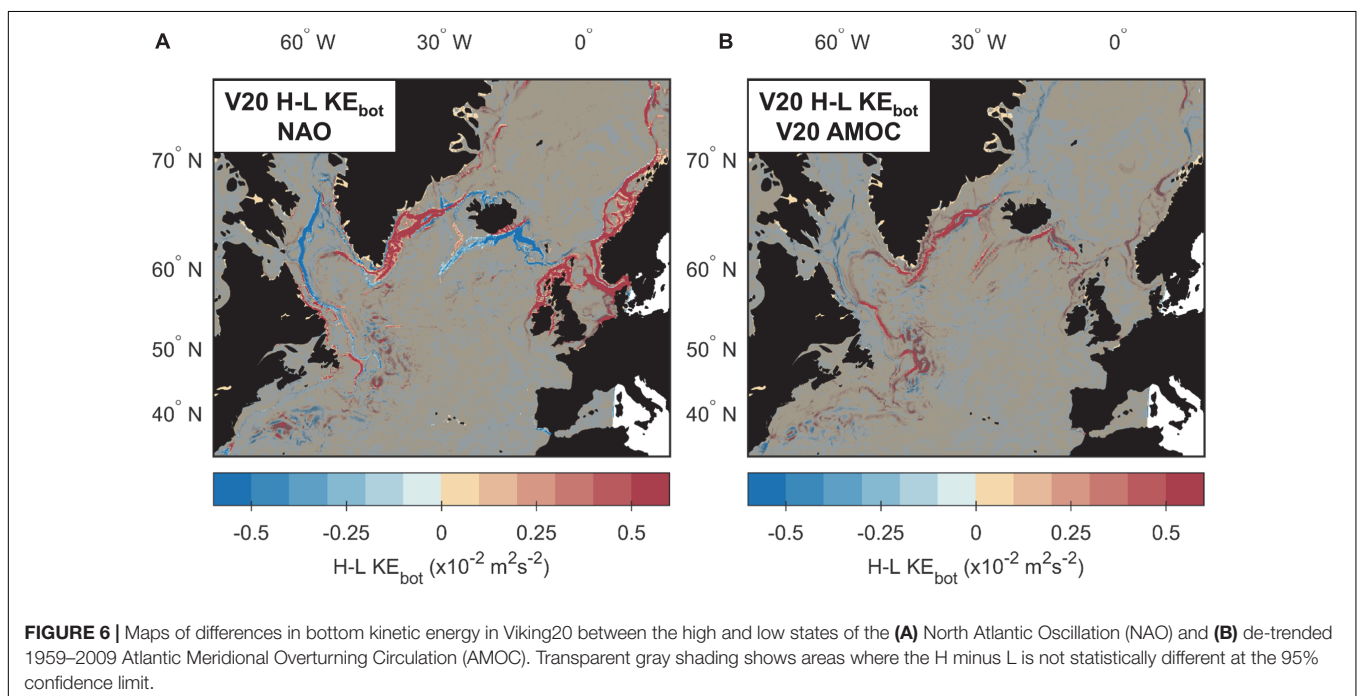
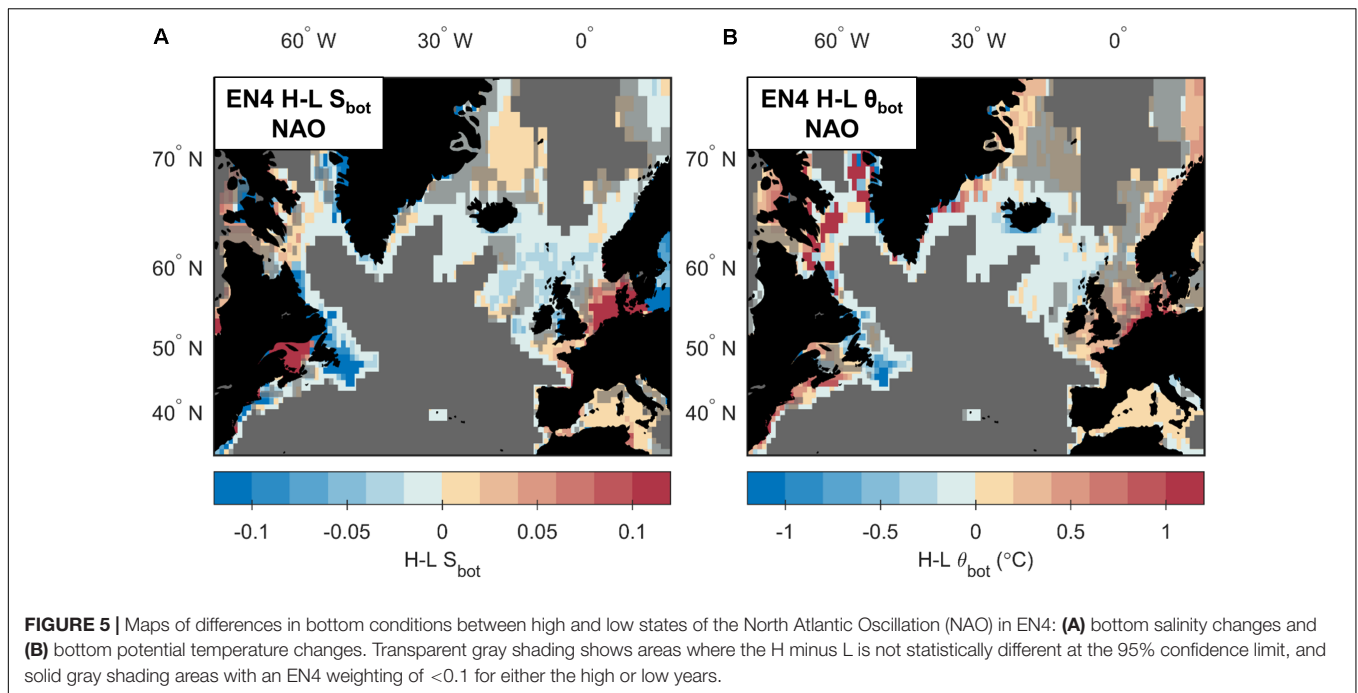
As the timing of changes in strength between the observational and modeled AMOC compare extremely well during the contemporaneous period (Figures 2B,F), we now use the de-trended Viking20 AMOC time-series to interrogate the EN4 dataset (Figures 7C,D). Applying the Viking20 AMOC time-series to the EN4 data assumes that the relationship between the observed and modeled AMOC persists outside the post-1993 era. However, the advantage is that it increases the amount of observational data used in the construction of the composites (Table 2) therefore increasing the spatial extent of the analysis.

Many spatial features observed in the composites created using the observed AMOC time-series (Figures 7A,B), are also seen in those created from the de-trended Viking20 AMOC time-series (Figures 7C,D). However, the magnitude of changes are often lower in the model AMOC composites. The extended selection period for the ocean observations is particularly noticeable in the relatively data-sparse areas deeper than 2000 m. Changes in bottom conditions are now revealed in the central Labrador and Irminger Seas, and for areas between approximately 40–52°N, which in the observational AMOC composite had a mean EN4 weighting of <0.1 and were therefore grayed out. Bottom conditions in the central Labrador Sea and Irminger Sea are also cooler (<-0.02) and fresher ($<-0.2^\circ\text{C}$) during a high AMOC. While fresher conditions are seen south of approximately 52°N, warmer θ_{bot} values are seen in western areas.

Finally, we use Viking20 and the modeled AMOC time-series to examine changes in KE_{bot} . We present a high minus low map created from the longer de-trended time-series (Figure 6B), which is very similar to the composite compiled from the post-1993 time-series in Viking20 (not shown). Stronger bottom currents are seen around the northern and western boundaries of the subpolar gyre as well as around Grand Banks. KE_{bot} in these areas is $0.5\text{--}1.5 \times 10^{-2} \text{ m}^2\text{s}^{-2}$ greater during a high AMOC than a low state. Although changes are seen along the European and Norwegian Slopes, these are not statistically significant.

Atlantic Multi-decadal Oscillation (AMO)

As discussed in section Climate Indices, it is not appropriate to apply the AMO time-series to output from Viking20; thus we examine changes using the EN4 dataset only and do not discuss KE_{bot} . High minus low values for the AMO are positive on the North American, Western European, and Greenland Shelves (Figure 8), with bottom conditions 0.6–1.0°C warmer and 0.02–0.2 more saline during a high AMO. Warmer and saltier conditions are also seen over the shallower Greenland-Scotland Ridge where S_{bot} and θ_{bot} are up to 0.8°C

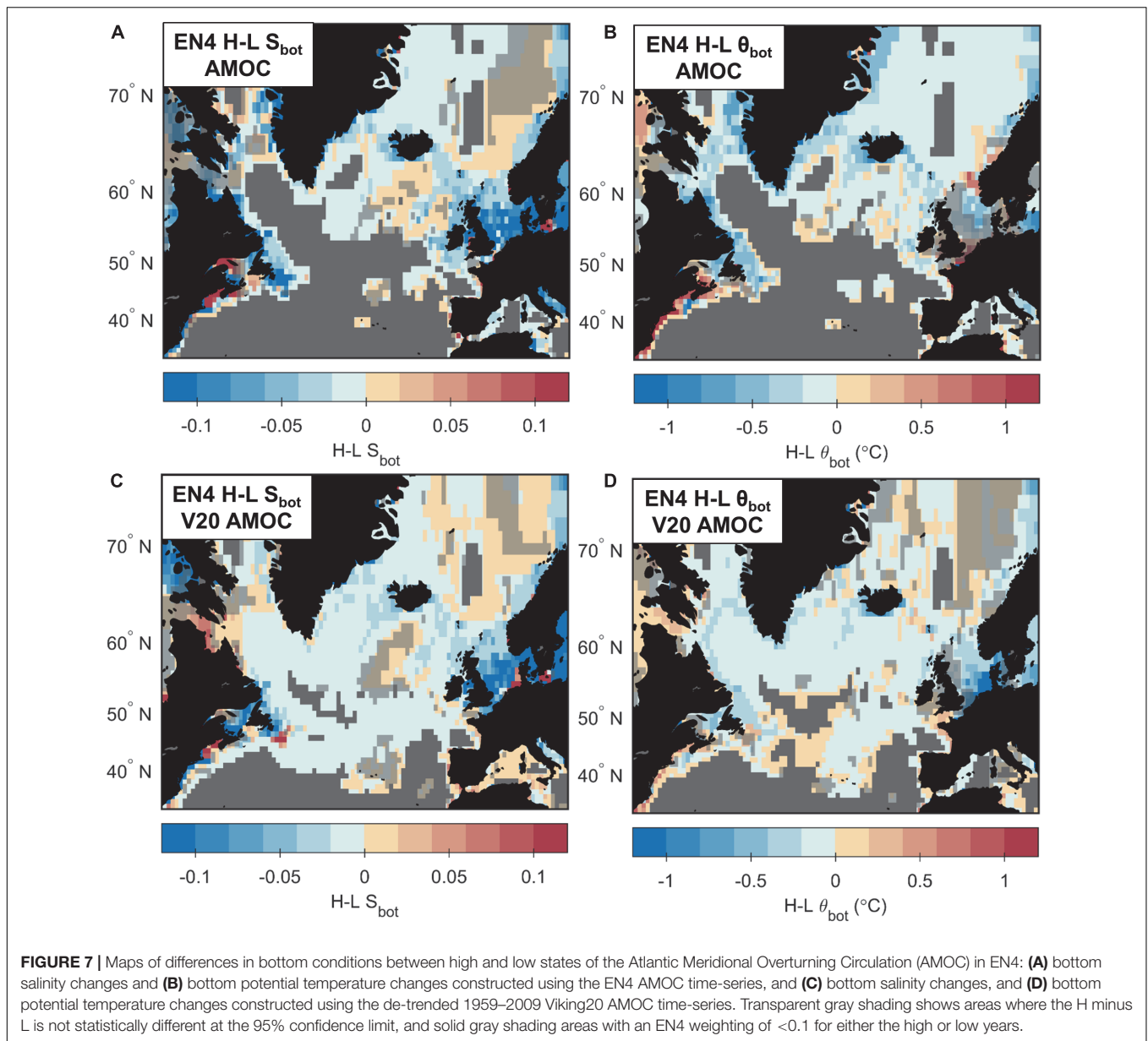


warmer during a high AMO state relative to a low AMO state, and up to 0.06 more saline. In regions deeper than 2000 m, there is a split between areas north and south of the Greenland-Scotland Ridge. In the deep Nordic Seas, θ_{bot} and S_{bot} are higher during a high AMO. In contrast, cooler and less saline bottom conditions are seen below approximately 2000 m in the northern North Atlantic. The magnitude of the changes in θ_{bot} and S_{bot} in both these regions are ± 0 –0.02 and ± 0 –0.2°C respectively. There is insufficient data to

assess any changes in areas deeper than 2000 m south of around 45–50°N.

Subpolar Gyre (SPG)

For the SPG, we again only examine changes in the EN4 dataset. Bottom conditions are cooler and fresher during a high SPG for the vast majority of the northern North Atlantic region regardless of bathymetric depth (**Figure 9**). On the continental shelves, lower S_{bot} values are seen on the North American (–0.15

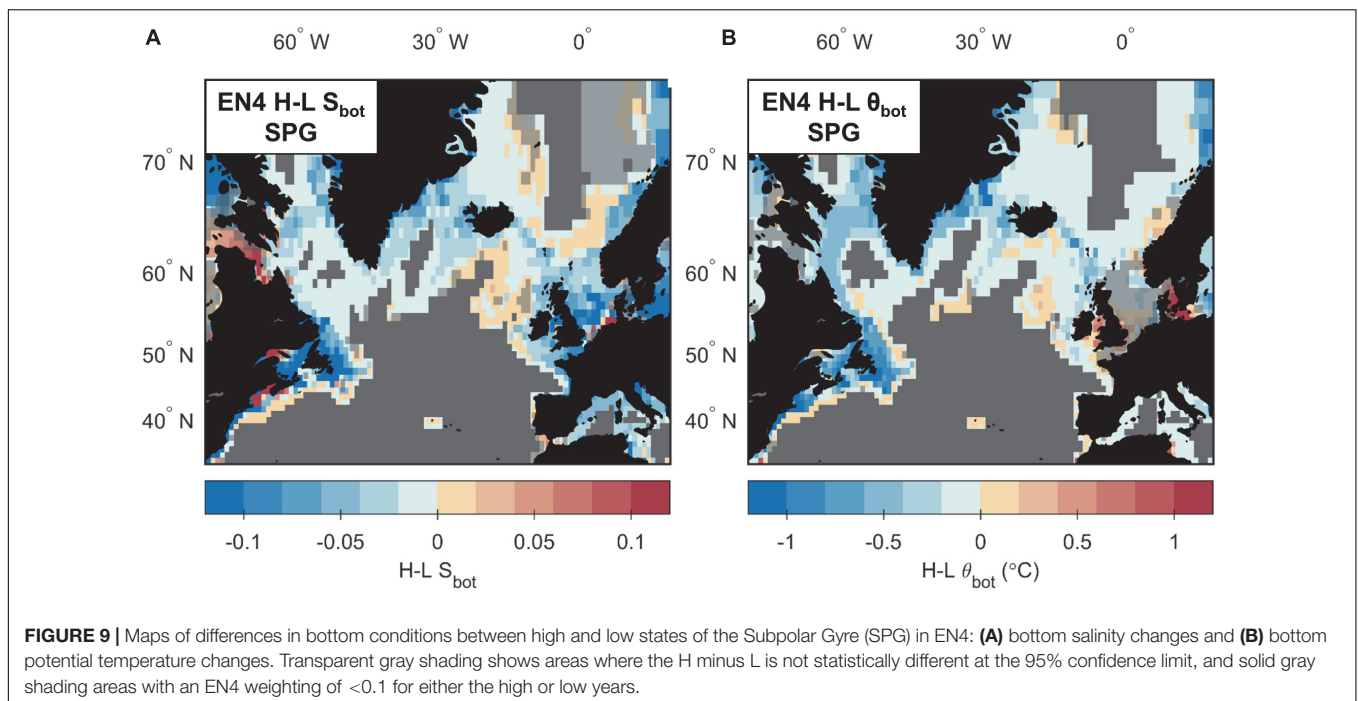
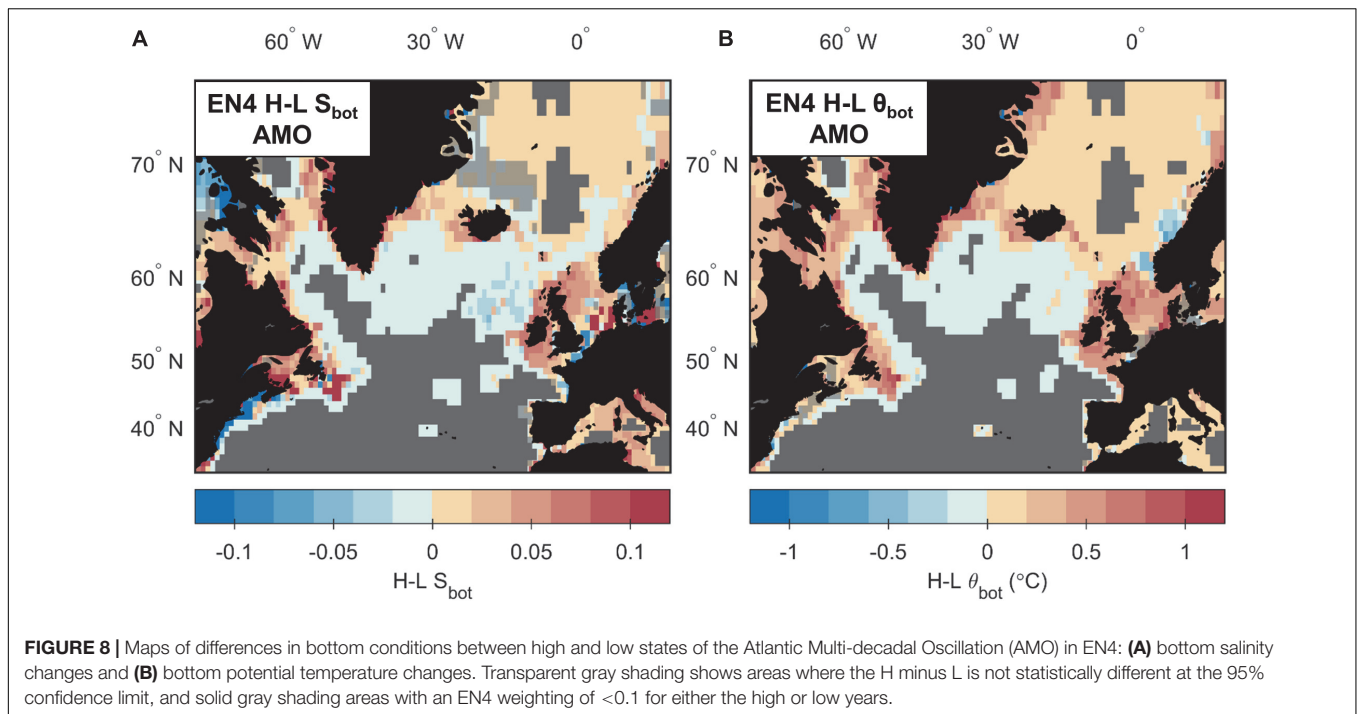


to -0.50), European (-0.04 to -0.25) and Norwegian Shelves (-0.04 to -0.08). However, decreased θ_{bot} values are observed only on the North American shelf (-0.8 to -1.5°C) with the absence of a cooling in the North Sea. On the Norwegian Shelf, cooler bottom waters are only seen north of approximately 70°N , even though the change in S_{bot} is widespread. Hence, whilst S_{bot} and θ_{bot} co-vary on the North American Shelf, this relationship does not exist in the North Sea and Norwegian Shelf. Despite the lack of a statistically robust temperature signal in the North Sea, lower θ_{bot} values (-0.2 to -0.8°C) are still observed on the European Shelf west of Scotland during a high SPG.

Away from the continental shelves, fresher and cooler conditions are observed in the majority of areas during a high SPG. Changes are particularly pronounced around the boundaries of the Labrador and Irminger Seas, and over the

Reykjanes and Greenland-Scotland Ridges. In these areas, bottom conditions are -0.02 to -0.06 fresher during a high SPG, relative to a low SPG, and -0.2 to -0.8°C colder. Cooler (0 to -0.1°C) and fresher (0 to -0.01) conditions are also observed in areas of the Labrador and Irminger Seas deeper than 2000 m, although these changes are smaller than those observed at the boundaries. In the eastern subpolar gyre, there are some areas of higher θ_{bot} and S_{bot} . In particular, bottom conditions in the Iceland Basin and Rockall Trough are up to 0.015 more saline during a high SPG than a low SPG. North of the Greenland-Scotland Ridge, the majority of the Nordic Seas show lower θ_{bot} values during a high SPG. However, again there are areas of more saline S_{bot} values, mainly in the eastern portions of the region.

Finally, we note that the pattern of changes in S_{bot} and θ_{bot} seen between the high and low states of the SPG (**Figure 9**),

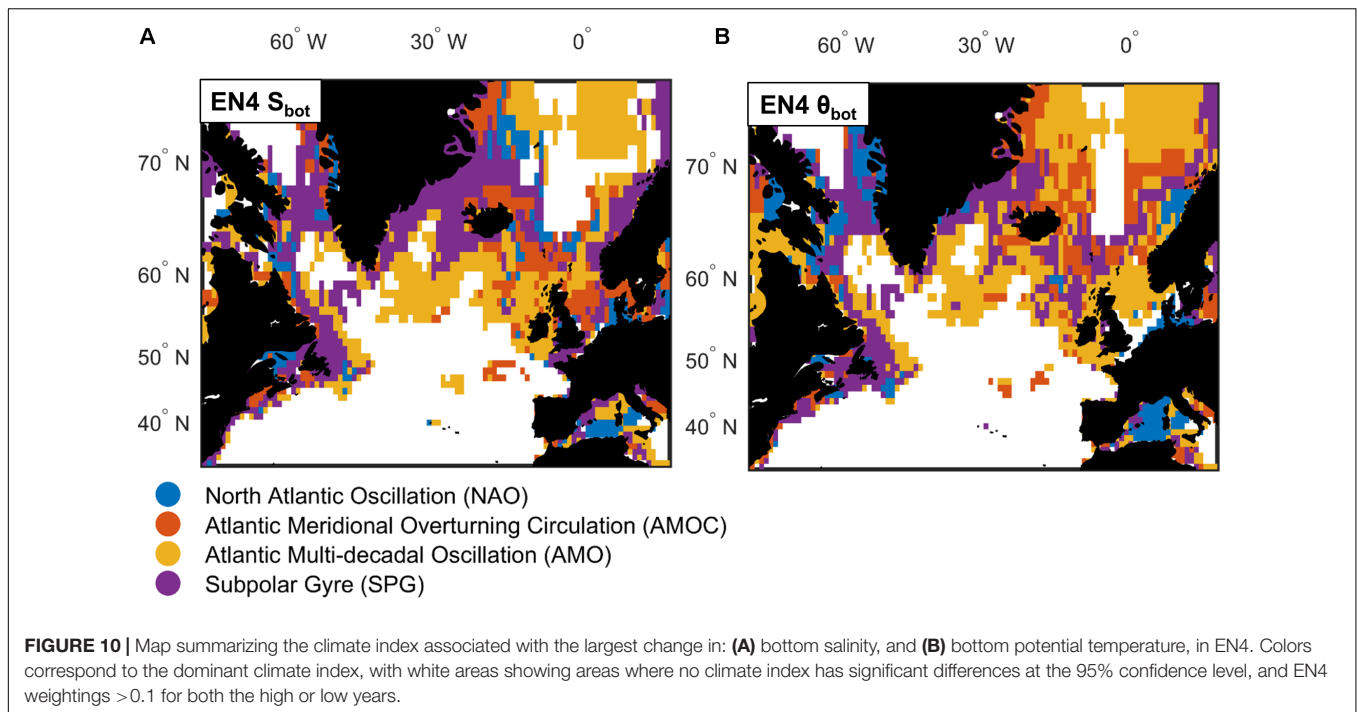


are very similar to that seen for the AMOC; particularly when considering the post-1993 AMOC time-series (**Figures 7A,B**). Although this may reflect a link between the two climate indices, the selection periods for the two indices are very similar (**Figure 2F**): the months used to create the high SPG average are almost identical to those used to create the post-1993 high AMOC composite, whilst the input periods for the low composites are sequential to each other. This suggests that a similar signal may be

represented for both indices, and thus it is hard to define whether the observed changes are dominated by the SPG, or the AMOC, or indeed whether the two indices act in unison.

Comparison Between Indices

We now examine the spatial dominance of each index by asking a simple question: which climate index is associated with the largest changes at each location? This enables us to examine



whether there are spatially coherent patterns, and how these vary both in the horizontal and vertical. As we have investigated more climate indices in EN4, we focus on the changes in S_{bot} and θ_{bot} . Again, we only consider changes that are statistically significant at the 95% confidence level, and where there is a weighting >0.1 for both the high and low composites. Although the patterns of variability for the AMOC and SPG are very similar, we include both indices separately to see if perhaps there is a spatial difference between the two.

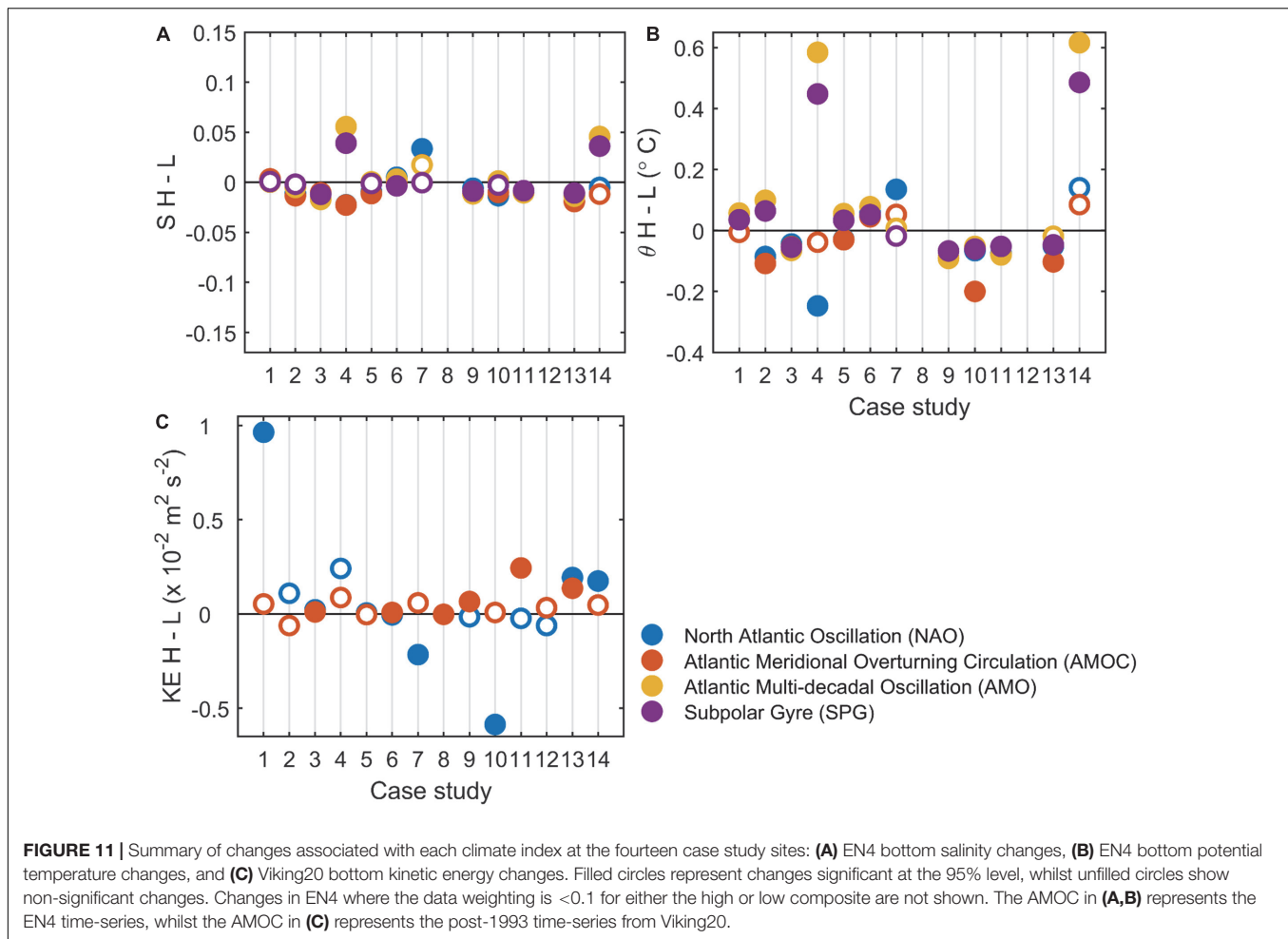
The dominant climate index pattern is reasonably similar for S_{bot} and θ_{bot} , although they are not identical (**Figure 10**). Whilst some areas are patchy, there are also some spatially coherent signals and general observations to be made. For example, where there is sufficient data to assess changes below 2000 m, the AMO is associated with the largest changes. This is true both in the Nordic Seas and northern North Atlantic. In contrast, the SPG dominates changes in areas shallower than 2000 m in the western subpolar North Atlantic, whilst the AMOC becomes more important in eastern areas. In the Mediterranean Sea, the NAO is associated with the largest changes, particularly when considering θ_{bot} . Changes on the North American Shelf are dominated by the SPG, whereas the shelf west of the UK is dominated by the AMO. In the North Sea the AMO also dominates changes in θ_{bot} , whilst the AMOC is more important for changes in S_{bot} .

RESULTS: VARIABILITY AT ECOSYSTEM CASE STUDY SITES

We now move on to discussing changes at fourteen case studies (**Figure 1** and **Table 1**) chosen to represent various VMEs across

the northern North Atlantic region. As these sites cover a number of management measures, such as ESBAs, MPAs, and VME closures, and are therefore often considered as a single entity, we show mean conditions averaged across each location. However, we caution that most case studies cover a range of depths (**Table 1**), which may be subject to different processes and signals, as well as lag periods. As such, changes at a particular depth may be different to the mean conditions for the entire case study site. For example, at Case Study 9 on the Reykjanes Ridge (**Figure 1**), the SPG is associated with the largest changes in S_{bot} in areas shallower than approximately 2000 m, whilst the largest changes in deeper areas are linked to the AMO (**Figure 10**). Additionally, if signals at different depths are opposing, changes averaged across the case study as a whole may be muted, despite statistically significant changes in individual depth layers. Similar effects will be produced in spatially heterogeneous areas, for example at case study 14 in the northern North Sea (**Figure 1**). Here, the AMOC is associated with the largest changes in S_{bot} in southern areas, whilst the largest changes in the northern part of the case study region is associated with the AMO (**Figure 10**). However, when the S_{bot} changes are averaged over the entire case study region, only the AMO is associated with statistically significant changes. Finally, as changes are often larger at shallower depths, case study averages are likely to be biased toward processes occurring higher in the water column. As such, we advise the reader to consider the results in this section in conjunction with Section Results: Spatial Variability Linked to Climate Indices and **Figures 5–10**.

We again use the EN4 dataset to examine changes in S_{bot} and θ_{bot} , and output from Viking20 to investigate changes in KE_{bot} although this is only for the NAO and AMOC. Time-series for each case study site are shown in



Supplementary Figures S5–S18, whilst changes between high and low climate states are summarized in **Figure 11** and **Tables 3, 4**. Again we consider the AMOC and SPG separately, and only describe changes in EN4 where the mean data weighting over the case study as a whole exceeds 0.1 for both the high and low states.

Case study 1 is situated on the Norwegian Coast. Here, only changes in θ_{bot} associated with the AMO and SPG are statistically significant at the 95% confidence level. Both indices show warmer θ_{bot} during high states, with the AMO having the largest change at 0.06°C . A large positive change in KE_{bot} ($0.96 \times 10^{-2} \text{ m}^2 \text{ s}^{-2}$) is also observed between high and low states of the NAO. At **case study 2**, on the western Scottish Slope, all climate indices are associated with significant changes in θ_{bot} . The NAO and AMOC have cooler θ_{bot} values during the high states, whilst the AMO and SPG show warmer θ_{bot} values. The NAO, AMOC, and AMO all produce similar magnitude changes. With respect to S_{bot} , only the NAO, AMOC, and AMO show statistically significant changes, with all having fresher S_{bot} values during a high state. The largest changes are associated with the AMOC (-0.013) and NAO (-0.011), with the change between high and low states of the AMO half of these values. No statistically significant changes in KE_{bot} are seen.

Case study 3 is at Rockall Bank. Here, changes in both θ_{bot} and S_{bot} are statistically significant for all climate indices. Cooler and fresher θ_{bot} and S_{bot} values are observed during high states. The largest change is associated with the AMO for both θ_{bot} (-0.07°C), and S_{bot} (-0.017). Changes in KE_{bot} though statistically significant are small ($0.01\text{--}0.02 \times 10^{-2} \text{ m}^2 \text{ s}^{-2}$). **Case study 4**, which has an average depth of 196 m and covers the Mingulay Reef complex to the west of Scotland (Roberts et al., 2009), shows large changes. Statistically significant changes in θ_{bot} are seen for the NAO, AMO, and SPG. The NAO has cooler θ_{bot} during a high state, whilst the AMO and SPG exhibit warmer θ_{bot} . All climate indices show significant changes in S_{bot} . The NAO and AMOC have less saline conditions during high states, and the AMO and SPG more saline S_{bot} values. The largest change in both θ_{bot} and S_{bot} is associated with the AMO (0.58°C and 0.056 respectively). Changes in KE_{bot} between high and low states of the NAO and AMOC are not statistically different at the 95% confidence level.

At **case study 5**, on the Porcupine Sea Bight, θ_{bot} shows statistically significant changes for all climate indices. Warmer θ_{bot} values are seen for high states of the NAO and AMOC, with lower θ_{bot} values seen during high states of the AMO and SPG. The largest change in θ_{bot} (0.06°C) is associated with the

TABLE 3 | Summary statistics from EN4 for the 14 case studies detailed in **Table 1**.

Case study	1959–2017 θ_{bot}			1959–2017 S_{bot}			NAO H-L		AMOC H-L		AMO H-L		SPG H-L	
	Mean (°C)	Min. (°C)	Max. (°C)	Mean	Min.	Max.	θ_{bot} (°C)	S_{bot}	θ_{bot} (°C)	S_{bot}	θ_{bot} (°C)	S_{bot}	θ_{bot} (°C)	S_{bot}
1	-1.01	-1.09	-0.92	34.913	34.876	34.954	-	-	-	-	0.06	-	0.04	-
2	-0.81	-1.07	-0.43	34.913	34.848	34.984	-0.09	-0.011	-0.11	-0.013	0.10	-0.005	0.06	-
3	3.62	3.47	3.79	34.969	34.926	35.019	-0.04	-0.010	-0.05	-0.011	-0.07	-0.017	-0.05	-0.012
4	9.54	8.19	11.05	35.375	35.254	35.460	-0.25	-0.022	-	-0.023	0.58	0.056	0.45	0.039
5	3.62	3.48	3.78	35.007	34.983	35.033	-0.03	-0.009	-0.03	-0.011	0.06	-	0.03	-
6	4.36	4.09	4.56	35.063	35.022	35.098	0.06	0.005	0.04	-	0.08	0.003	0.05	-0.003
7	9.40	8.87	10.08	36.000	35.771	36.203	0.14	0.034	-	-	-	-	-	-
8	2.40	2.36	2.49	34.929	34.911	34.946	-	-	-	-	-	-	-	-
9	2.90	2.69	3.07	34.952	34.915	34.988	-0.07	-0.006	-0.09	-0.012	-0.09	-0.012	-0.07	-0.009
10	3.22	2.95	3.54	34.912	34.877	35.000	-0.07	-0.013	-0.20	-0.010	-0.05	-	-0.06	-0.003
11	2.49	2.24	2.73	34.911	34.877	34.957	-0.07	-0.009	-0.08	-0.010	-0.08	-0.010	-0.05	-0.008
12	2.96	2.77	3.12	34.955	34.906	34.998	-	-	-	-	-	-	-	-
13	3.97	3.74	4.21	34.995	34.921	35.058	-0.05	-0.013	-0.10	-0.019	-	-0.014	-0.05	-0.011
14	7.59	5.89	9.35	35.174	34.838	35.407	-	-	-	-	0.62	0.046	0.49	0.036

Columns two and three contain the mean, minimum and maximum for bottom potential temperature and bottom salinity respectively between 1959 and 2017. All case studies have a mean weighting > 0.1 except case study 8 where the mean weighting is 0.098. Columns four to seven contain the differences in bottom conditions between high and low states of the North Atlantic Oscillation (NAO), Atlantic Meridional Overturning Circulation (AMOC), Atlantic Multi-decadal Oscillation (AMO) and Subpolar Gyre (SPG) respectively. Only differences that are statistically significant at the 95% confidence level, and where data weightings during both the high and low states are > 0.1 are shown. AMOC represents the EN4 time-series.

AMOC. Only the NAO and AMOC show statistically significant changes in S_{bot} , with the largest change again being associated with the AMOC (-0.011). Changes in KE_{bot} are not significant at the 95% level for either the NAO or AMOC. **Case study 6** is in the Bay of Biscay. Here, θ_{bot} shows statistically significant

changes for all climate indices, with warmer values observed during the high states. The largest change is associated with the AMO (0.08°C). Only the AMOC does not show a statistically significant change in S_{bot} between high and low states. The NAO and AMO have more saline S_{bot} during high states, with the SPG having lower S_{bot} values. The largest change is associated with the NAO although this is still small at 0.005. KE_{bot} changes, whilst significant, are small ($\pm 0.01 \times 10^{-2} \text{ m}^2 \text{ s}^{-2}$).

TABLE 4 | Summary statistics from Viking20 for the 14 case studies detailed in **Table 1**.

Case study	1959–2009 KE_{bot} ($\times 10^{-2} \text{ m}^2 \text{ s}^{-2}$)			NAO H-L KE_{bot} ($\times 10^{-2} \text{ m}^2 \text{ s}^{-2}$)	AMOC H-L KE_{bot} ($\times 10^{-2} \text{ m}^2 \text{ s}^{-2}$)
	Mean	Min.	Max.		
1	1.44	0.27	5.90	0.96	-
2	1.08	0.41	2.68	-	-
3	0.11	0.04	0.23	0.02	0.01
4	0.48	0.02	3.00	-	-
5	0.06	0.02	0.15	-	-
6	0.05	0.01	0.24	-	0.01
7	2.66	2.09	3.84	-0.22	-
8	0.02	0.01	0.06	-	0.00
9	0.38	0.21	0.61	-	0.07
10	2.09	0.39	3.98	-0.59	-
11	1.51	0.89	2.93	-	0.24
12	0.50	0.07	1.89	-	-
13	0.40	0.06	1.47	0.19	0.14
14	0.28	0.03	1.03	0.17	-

Column two contains the mean, minimum and maximum for bottom kinetic energy between 1959 and 2009. Columns three and four contain the differences in bottom conditions between high and low states of the North Atlantic Oscillation (NAO), and Atlantic Meridional Overturning Circulation (AMOC) respectively. Only differences that are statistically significant at the 95% confidence level are shown. AMOC represents the Viking20 post-1993 time-series.

Case study 7 is located in the Gulf of Cadiz and has a mean depth of 697 m. Here, only the NAO shows statistically significant changes in θ_{bot} and S_{bot} (0.14°C and 0.034 respectively). In Viking20, the NAO is also associated with weaker KE_{bot} ($-0.22 \times 10^{-2} \text{ m}^2 \text{ s}^{-2}$) during a high state. **Case study 8** is situated around the Azores and is the deepest site with a mean depth of 3064 m. There is insufficient observational data to assess changes here with EN4 weightings < 0.1 for all climate indices. Changes in KE_{bot} , as expected for a deep site away from boundary currents, are negligible.

At **case study 9**, which is situated on the Reykjanes Ridge, statistically significant changes are observed for all climate indices with both θ_{bot} and S_{bot} . All changes are negative with cooler and fresher bottom conditions during high states. The largest changes are associated with the AMO and AMOC, with both indices having changes of -0.09°C and -0.012 for θ_{bot} and S_{bot} respectively. Only the AMOC is associated with a small ($0.07 \times 10^{-2} \text{ m}^2 \text{ s}^{-2}$), but statistically significant positive change in KE_{bot} between high and low states. **Case study 10** is situated in the Davis Strait. All climate indices show statistically significant changes for θ_{bot} , with cooler conditions during a high state. The largest change is associated with the AMOC (-0.2°C), with this being over 0.1°C greater than changes for the NAO, AMO, and SPG. For S_{bot} the NAO, AMOC, and SPG all show statistically

significant changes in EN4 with fresher conditions during a high state. The changes associated with the NAO and AMOC are three to four times that of changes from the SPG, with the largest change associated with the NAO (-0.013). In Viking20, the NAO is associated with less energetic conditions ($-0.59 \times 10^{-2} \text{ m}^2 \text{ s}^{-2}$) during a high state.

Case study 11, which is situated on the Flemish Cap, shows statistically significant changes with both θ_{bot} and S_{bot} for all climate indices, with cooler and fresher conditions during high states. The largest change in θ_{bot} is associated with the AMOC and AMO, with both indices showing a change of -0.08°C . However, the NAO shows only a slightly smaller change of -0.07°C . All changes in S_{bot} exceed -0.008 , with the largest change of -0.010 again associated with the AMOC and AMO. KE_{bot} shows more energetic conditions ($0.24 \times 10^{-2} \text{ m}^2 \text{ s}^{-2}$) during a high AMOC. **Case study 12**, covering the USA mid-Atlantic Canyons, has a lack of observational data with EN4 weightings <0.1 for all climate indices. Additionally, changes in KE_{bot} are not statistically significant.

At **case study 13**, on the European Slope, the NAO, AMOC, and SPG all show statistically significant changes with θ_{bot} , with cooler conditions during high states. The largest change is associated with the AMOC (-0.1°C), with this being twice the size of changes from the NAO and SPG. With respect to S_{bot} , all climate indices show a statistically significant change in EN4 with fresher conditions during a high state. The largest change in S_{bot} is again associated with the AMOC (-0.019). Both the NAO and AMOC are associated with enhanced KE_{bot} ($>0.14 \times 10^{-2} \text{ m}^2 \text{ s}^{-2}$) during high states. **Case study 14** is in the North Sea and is the shallowest site with a mean depth of 99 m. Only the AMO and SPG show statistically significant changes with both θ_{bot} and S_{bot} . Warmer and more saline bottom conditions are seen during high states, with the largest changes for both parameters associated with the AMO (0.62°C and 0.046). In Viking20, a statistically significant change in KE_{bot} ($0.17 \times 10^{-2} \text{ m}^2 \text{ s}^{-2}$) is associated with the NAO.

DISCUSSION

In this paper, we set out to ask whether there are statistically significant changes in bottom conditions across the northern North Atlantic, and its adjacent shelf seas, associated with four major climate indices, and whether these changes are spatially coherent. The answer to both of these questions is “yes,” but what of the physical processes responsible for these changes? This is a more nuanced question. Bottom conditions in the northern North Atlantic region span shallow seas to deep oceans; thus in one map we have contrasting dynamical regimes: from highly seasonal shelf seas, and energetic boundary currents, to quiescent abyssal depths. It is likely that different mechanisms are important at different depths, and lag-times between changes in the index and bottom manifestations will also vary. In this discussion section, we touch on some possible physical processes responsible for observed significant correlations, but anticipate that we only scratch the surface leaving deeper analysis for future work.

North Atlantic Oscillation (NAO)

The NAO shows a strong anti-correlation between the eastern and western continental shelves (**Figure 5**): warmer and more saline bottom conditions are seen in the North Sea during a high NAO, with cooler and fresher conditions in the Grand Banks area. The higher θ_{bot} observed in the North Sea during a high NAO, is likely a representation of the higher sea surface temperatures seen in the same region during a positive NAO (Visbeck et al., 2013) due to the tidally well-mixed water column (e.g., Huthnance, 1991). Bottom kinetic energy is higher during a high NAO along the European and Norwegian Shelf break, and along flow pathways into the North Sea (**Figure 6A**). This reduction in the European Slope Current strength in Viking20 during a low NAO, is consistent with evidence of a slowing of the slope current during the 1990’s attributed to changes in both the wind-field and the meridional oceanic density gradient (Marsh et al., 2017). Similar changes are observed in the Norwegian Slope Current with enhanced transport during a high NAO (Skagseth et al., 2004).

Away from the continental shelves, lower S_{bot} and θ_{bot} values are observed in the subpolar gyre during a high NAO (**Figure 5**). Convection in the Labrador Sea is enhanced during a high NAO producing cooler and fresher Labrador Sea Water (Yashayaev, 2007). In contrast, convection in the Nordic Seas is reduced during a high NAO resulting in warmer and more saline bottom waters (Dickson et al., 1996; Alekseev et al., 2001). This may explain the cooler and fresher bottom conditions in the Labrador and Irminger Seas. Advection times of Labrador Sea Water to the eastern subpolar regions are in the order of 5–10 years (Yashayaev et al., 2007a,b). This suggests that there may be periods where properties of the Labrador Sea Water in the western subpolar North Atlantic may be out of phase to those in eastern areas. However, the temporal spacing between high and low years in the NAO time-series exceeds this, and we see cooler and fresher conditions during a high NAO right across the subpolar latitudes.

Finally, we see no evidence of the saltier Iceland Scotland Overflow Water during a high NAO observed by Sarafanov (2009), although this is not unexpected for EN4 due to its low horizontal resolution relative to the overflow waters spatial extent. We do, however, see reduced mean KE_{bot} in the Iceland-Scotland Overflow during a high NAO, with coincident increased KE_{bot} in the Denmark Strait Overflow region (**Figure 6A**). Less vigorous flow in Iceland-Scotland Overflow Water during a high NAO is consistent with results from a sediment core on the eastern flank of the Reykjanes Ridge (Boessenkool et al., 2007). Additionally, the anti-correlation between the eastern and western overflow branches is consistent with previous work that shows overflow volume transports are correlated with NAO-type changes in sea level pressure and wind stress curl, and that transports between the eastern and western routes can be out of phase (Biaostoch et al., 2003; Bringedal et al., 2018).

Atlantic Meridional Overturning Circulation (AMOC)/Subpolar Gyre (SPG)

As mentioned, the composites produced using the post-1993 AMOC time-series (**Figures 7A,B**), and those produced using

the SPG time-series (**Figure 9**) are very similar; probably reflecting the similar time-periods used in the construction of the composites (**Figure 2F**). As such, it is difficult to tease out whether the AMOC, or the SPG, is the most dominant index, or indeed whether the two indices act in unison. We therefore discuss both indices together here. Cooler and fresher bottom conditions are seen in the western subpolar North Atlantic during a high AMOC/SPG, with pronounced changes around the boundaries of the Labrador Sea, and over the Reykjanes and Greenland-Scotland Ridges (**Figures 7, 9**). Lower θ_{bot} and S_{bot} values are also seen over the Rockall-Hatton Plateau and on the continental shelf west of the UK during a high AMOC/SPG, although more saline conditions are seen in the Rockall Trough and Iceland Basin.

Upper ocean properties show a dipole pattern for the AMOC. During a high AMOC, cooler conditions are seen in the Gulf Stream region, and warmer conditions in the subpolar North Atlantic (Zhang, 2008; Tulloch and Marshall, 2012; Caesar et al., 2018). As such, we may expect to see similar changes in θ_{bot} in shallower areas which are influenced by the upper waters. However, we see no evidence of this; indeed, shallower areas of the subpolar gyre show cooler (and fresher) conditions (**Figure 7**). This may be because the relationship between upper ocean heat content changes and the AMOC is thought to reflect processes that act on multi-decadal time-scales (Kushnir, 1994; Zhang, 2008), whereas our analysis focusses on multi-annual variability. An alternative possibility is that the SPG dominates upper ocean properties (**Figure 9**). Upper water properties in the eastern and central subpolar North Atlantic are negatively correlated with the SPG (Holliday, 2003; Hátún et al., 2005; Johnson et al., 2013). Whilst at deeper levels, the SPG has also been shown to effect the eastward extent of Labrador Sea Water (Lozier and Stewart, 2008), as well as the northward limit of Mediterranean Overflow Water (Lozier and Stewart, 2008; Bozec et al., 2011).

By definition, a high AMOC indicates a stronger overturning circulation with increased northward flow of upper waters and a similar increase in the return flow of deep waters. Additionally, it specifies enhanced conversion of upper waters to denser waters either in the subpolar gyre and/or Nordic Seas. As expected, KE_{bot} is higher in the northern and western boundaries of the subpolar gyre during a high AMOC (**Figure 6B**), suggesting more energetic flow in the overflow currents and deep western boundary current. These areas also see a lower θ_{bot} and S_{bot} during a high AMOC, which we speculate may be linked to enhanced flow of cooler and fresher dense waters around the subpolar gyre. Although the KE_{bot} composite was created using the AMOC time-series, we also expect this variable to be effected by the SPG as more energetic flows have been observed during a high state (Häkkinen and Rhines, 2004).

Atlantic Multi-decadal Oscillation (AMO)

Spatial changes associated with the AMO are relatively simple (**Figure 8**). Warmer and more saline bottom conditions are observed: around the boundaries of the northern North Atlantic, on the continental shelves, in the Mediterranean Sea, and in

the Nordic Seas during a high state. In contrast, cooler and fresher θ_{bot} and S_{bot} are seen in areas deeper than around 2000 m in the northern North Atlantic. The AMO shows a strong positive correlation with ocean heat content changes in the upper 700 m averaged over 45–70°N (Frajka-Williams et al., 2017). As such, it does not seem surprising that areas influenced by upper waters, such as the boundaries of the subpolar gyre and continental shelves, are warmer during a high AMO state. The high AMO years are seen post-1998, whilst the low AMO years are between 1970 and 1994 (**Figure 2D**). Therefore, it is possible that our results represent the global increase in ocean heat content over the past half a century (e.g., Levitus et al., 2012), rather than a signal of the AMO. Although we cannot discount this influence, the fact that bottom temperature and salinity co-vary over the vast majority of the northern North Atlantic region (**Figure 8**), suggests that our composites reflect a process other than just a simple long-term warming. The spatially coherent and statistically significant changes in S_{bot} and θ_{bot} in the deeper northern North Atlantic and Nordic Seas are intriguing. Whilst changes at shallower depth levels and deeper areas are in phase in the Nordic Seas, they appear to be anti-correlated in the northern North Atlantic; that is, during a high AMO the shallower boundaries of the northern North Atlantic are warmer and more saline, whilst the deep interior is cooler and fresher.

CONCLUSION

Our results are the first to examine changes in bottom conditions across the northern North Atlantic Ocean, and its adjacent shelf seas, associated with four major climate indices. We show statistically significant and spatially coherent patterns of change between high and low states of the NAO, AMOC, AMO, and SPG. Although variations in bottom conditions are relatively small, due to the multi-annual nature of the climate indices any associated change may persist for several years. As such, vulnerable deep-sea ecosystems may be exposed to sustained changes in mean conditions, with this deviation in the baseline also altering the likelihood of extreme events such as marine heat waves. Any changes have the potential to effect sessile deep-sea ecosystems to a greater extent than more mobile pelagic species. Additionally, natural changes will be superimposed on any anthropogenic effects, exacerbating or moderating the impact on possibly stressed ecosystems. Thus, a thorough understanding of natural variability is essential for the evaluation of future scenarios and the implementation of management frameworks. Our work provides a first look at the signature of natural variability on benthic conditions in the northern North Atlantic region; we hope that this stimulates further work both on the physical mechanisms and potential effects on deep-sea ecosystems.

DATA AVAILABILITY STATEMENT

The datasets generated for this study are available on request to the corresponding author.

AUTHOR CONTRIBUTIONS

SG extracted the bottom data from Viking20, and MI the bottom data from EN4. CJ carried out the bulk of the analysis and prepared the first draft of the manuscript. All authors contributed to the conception and design of the study, manuscript revision, and read and approved the submitted version.

FUNDING

This project has received funding from the European Union's Horizon 2020 Research and Innovation Programme under grant agreement nos. 678760 (ATLAS), 633211 (AtlantOS), 818123 (iAtlantic), and 727852 (Blue-Action). This output reflects only the author's view and the European Union cannot be held responsible for any use that may be made of the information contained therein. MI received funding from UK NERC AlterEco

REFERENCES

- Alekseev, G., Johannessen, O., Korabiev, A., Ivanov, V., and Kovalevsky, D. (2001). Interannual variability in water masses in the Greenland Sea and adjacent areas. *Polar Res.* 20, 201–208. doi: 10.3402/polar.v20i2.6518
- Behrens, A., Våge, K., Harden, B., Biastoch, A., and Böning, C. (2017). Composition and variability of the Denmark Strait Overflow Water in a high-resolution numerical model hindcast simulation. *J. Geophys. Res. Oceans* 122, 2830–2846. doi: 10.1002/2016JC012158
- Berx, B., and Payne, M. (2017). The subpolar Gyre Index – a community data set for application in fisheries and environmental research. *Earth Syst. Sci. Data* 9, 259–266. doi: 10.5194/essd-9-259-2017
- Biastoch, A., Käse, R., and Stammer, D. (2003). The sensitivity of Greenland-Scotland Ridge overflow to forcing changes. *J. Phys. Oceanogr.* 33, 2307–2319. doi: 10.1175/1520-04852003033<2307:TSOTGR>2.0.CO;2
- Boessenkool, K., Hall, I., Elderfield, H., and Yashayaev, I. (2007). North Atlantic climate and deep-ocean flow speed changes during the last 230 years. *Geophys. Res. Lett.* 34:L13614. doi: 10.1029/2007GL030285
- Bozec, A., Lozier, S., Chassignet, E., and Halliwell, G. (2011). On the variability of the Mediterranean Overflow Water in the North Atlantic from 1948 to 2006. *J. Geophys. Res. Oceans* 116:C09033. doi: 10.1029/2011JC007191
- Breckenfelder, T., Rhein, M., Roessler, A., Böning, C., Biastoch, A., Behrens, E., et al. (2017). Flow paths and variability of the North Atlantic Current: a comparison of observations and a high-resolution model. *J. Geophys. Res. Oceans* 122, 2686–2708. doi: 10.1002/2016JC012444
- Bringedal, C., Eldevik, T., Skagseth, Ø, Spall, M., and Østerhus, S. (2018). Structure and forcing of observed changes across the Greenland-Scotland Ridge. *J. Clim.* 31, 9881–9901. doi: 10.1175/JCLI-D-17-0889.1
- Buckley, M., and Marshall, J. (2016). Observations, inferences and mechanisms of Atlantic Meridional Overturning Circulation variability: a review. *Rev. Geophys.* 54, 5–63. doi: 10.1002/2015RG000493
- Böning, C., Behrens, A., Getzlaff, K., and Bamber, J. (2016). Emerging impact of greenland meltwater on deepwater formation in the North Atlantic ocean. *Nat. Geosci.* 9, 523–527. doi: 10.1038/NNGEO2740
- Caesar, L., Rahmstorf, S., Robinson, A., Feulner, G., and Saba, V. (2018). Observed fingerprint of a weakening Atlantic ocean overturning circulation. *Nature* 556, 191–196. doi: 10.1038/s41586-018-0006-5
- Chafik, L., Nilsen, J., Dangendorf, S., Reverdin, G., and Frederikse, T. (2019). North Atlantic ocean circulation and decadal sea level change during the altimetry era. *Nat. Sci. Rep.* 9:1041. doi: 10.1038/s41598-018-37603-6
- Debreu, L., Vouland, C., and Blayo, E. (2008). AGRIF: adaptive grid refinement in fortran. *Comput. Geosci.* 31, 8–13. doi: 10.1016/j.cageo.2007.01.009
- Dickson, R., Lazier, J., Meincke, J., Rhines, P., and Swift, J. (1996). Long-term coordinated changes in the convective activity of the North Atlantic. *Prog. Oceanogr.* 38, 241–295. doi: 10.1016/S0079-6611(97)00002-5

(Grant No. NE/P013902/1) and SC received funding from UK NERC OSNAP (Grant No. NE/K010700/1).

ACKNOWLEDGMENTS

We thank Arne Biastoch and Erik Behrens for the use of Viking20 output, and for extracting the velocities perpendicular to the OSNAP-EAST line from Viking20. We also thank Matt Toberman for compiling the EN4 data. We thank the reviewers for their time and thoughtful comments.

SUPPLEMENTARY MATERIAL

The Supplementary Material for this article can be found online at: <https://www.frontiersin.org/articles/10.3389/fmars.2020.00002/full#supplementary-material>

- Enfield, D., Mestas-Nunez, A., and Trimble, P. (2001). The Atlantic multidecadal oscillation and its relationship to rainfall and river flows in the continental United States. *Geophys. Res. Lett.* 28, 2077–2080. doi: 10.1029/2000GL012745
- Etourneau, J., Sgubin, G., Crosta, X., Swingedouw, D., Willmott, V., Barbara, L., et al. (2019). Ocean temperature impact on ice shelf extend in the eastern Antarctic Peninsula. *Nat. Commun.* 10, 304. doi: 10.1038/s41467-018-08195-6
- Frajka-Williams, E., Beaulieu, C., and Duchez, A. (2017). Emerging negative Atlantic multidecadal oscillation index in spite of warm subtropics. *Nat. Sci. Rep.* 7:11224. doi: 10.1038/s41598-017-11046-x
- Gary, S., Cunningham, S., Johnson, C., Houpert, L., Holliday, N., Behrens, E., et al. (2018). Seasonal cycles of oceanic transports in the eastern subpolar North Atlantic. *J. Geophys. Res. Oceans* 123, 1471–1484. doi: 10.1002/2017JC013350
- Good, S., Martin, M., and Rayner, N. (2013). EN4: quality controlled ocean temperature and salinity profiles and monthly objective analyses with uncertainty estimates. *J. Geophys. Res. Oceans* 118, 6704–6716. doi: 10.1002/2013JC009067
- Häkkinen, S., and Rhines, P. (2004). Decline of the subpolar North Atlantic circulation during the 1990s. *Science* 304, 555–559. doi: 10.1126/science.1094917
- Häkkinen, S., Rhines, P., and Worthern, D. (2011). Atmospheric blocking and Atlantic multidecadal ocean variability. *Science* 334, 655–659. doi: 10.1126/science.1205683
- Häkkinen, S., Rhines, P., and Worthern, D. (2013). Northern North Atlantic sea surface height and ocean heat content variability. *J. Geophys. Res. Oceans* 118, 3670–3678. doi: 10.1002/jgrc.20268
- Handmann, P., Fischer, J., Visbeck, M., Karstensen, J., Biastoch, A., Böning, C., et al. (2018). The Deep Western boundary current in the Labrador Sea from observations and a high-resolution model. *J. Geophys. Res. Oceans* 123, 2829–2850. doi: 10.1002/2017JC013702
- Hátún, H., Sando, A., Drange, H., Hansen, B., and Valdimarsson, H. (2005). Influence of the Atlantic subpolar gyre on the thermohaline circulation. *Science* 309, 1841–1844. doi: 10.1126/science.1114777
- Holliday, N. P. (2003). Air-sea interaction and circulation changes in the northeast Atlantic. *J. Geophys. Res. Oceans* 108, 2156–2202. doi: 10.1029/2002JC001344
- Hurrell, J. W. (1995). Decadal trends in the North Atlantic Oscillation: regional temperatures and precipitation. *Science* 269, 676–679. doi: 10.1126/science.269.5224.676
- Huthnance, J. (1991). Physical oceanography of the North Sea. *Ocean Shoreline Manag.* 16, 199–231.
- Johnson, C., Inall, M., and Häkkinen, S. (2013). Declining nutrient concentrations in the northeast Atlantic as a result of a weakening subpolar Gyre. *Deep Sea Res.* 182, 95–107. doi: 10.1016/j.dsr.2013.08.007
- Johnson, D., Ferreira, M., and Kenchington, E. (2018). Climate change is likely to severely limit the effectiveness of deep-sea ABMTs in the North Atlantic. *Mar. Policy* 87, 111–122. doi: 10.1016/j.marpol.2017.09.034

- Jones, P., Jónsson, T., and Wheeler, D. (1997). Extension to the North Atlantic Oscillation using early instrumental pressure observations from Gibraltar and South-West Iceland. *Int. J. Climatol.* 17, 1433–1450. doi: 10.1002/(SICI)1097-0088(199711)17
- Kerr, R. (2000). A North Atlantic pacemaker for the centuries. *Science* 288, 1984–1985. doi: 10.1126/science.288.5473.1984
- Kushnir, Y. (1994). Interdecadal variations in North Atlantic sea surface temperatures and associated atmospheric conditions. *J. Clim.* 7, 141–157. doi: 10.1175/1520-04421994007<0141:IVINAS>2.0.CO;2
- Large, W., and Yeager, S. (2009). The global climatology of an interannually varying air-sea flux data set. *Clim. Dyn.* 33, 341–364. doi: 10.1007/s00382-008-0441-3
- Levitus, S., Antonov, J., Boyer, T., Baranova, O., Garcia, H., Locarnini, R., et al. (2012). World ocean heat content and thermosteric sea level change (0–2000 m), 1955–2010. *Geophys. Res. Lett.* 39, 1–5. doi: 10.1029/2012GL051106
- Lozier, M. (2010). Deconstructing the conveyor belt. *Science* 328, 1507–1511. doi: 10.1126/science.118925
- Lozier, M., Li, F., Bacon, S., Bahr, F., Bower, A., Cunningham, S., et al. (2019). A sea change in our view of overturning in the subpolar North Atlantic. *Science* 363, 516–521. doi: 10.1126/science.aau6592
- Lozier, M., and Stewart, N. (2008). On the temporally-varying northward penetration of Mediterranean Overflow Water and eastward penetration of Labrador Sea Water. *J. Phys. Oceanogr.* 38, 2097–2103. doi: 10.1175/2008JPO3908.1
- Marsh, B., Haigh, I., Cunningham, S., Inall, M., Porter, M., and Moat, B. (2017). Large-scale forcing of the European Slope Current and associated inflows to the North Sea. *Ocean Sci.* 13, 315–335. doi: 10.5194/os-13-315-2017
- Marshall, J., Kushnir, Y., Battisti, D., Chang, P., Cxaja, A., Dickson, R., et al. (2001). Review: North Atlantic climate variability: phenomena, impacts and mechanisms. *Int. J. Climatol.* 21, 1863–1898. doi: 10.1002/joc.693
- Mercier, H., Lherminier, P., Sarafanov, A., Gaillard, F., Daniault, N., Desbruyères, D., et al. (2015). Variability of the meridional overturning circulation at the Greenland-Portugal OVIDE section from 1993 to 2010. *Prog. Oceanogr.* 132, 250–261. doi: 10.1016/j.pocean.2013.11.001
- Mertens, C., Rhein, M., Walter, M., Böning, C., Behrens, E., Kieke, D., et al. (2014). Circulation and transport in the Newfoundland Basin, western subpolar North Atlantic. *J. Geophys. Res. Oceans* 119, 7772–7793. doi: 10.1002/2014JC010019
- Morato, T., Pham, C., Pinto, C., Goulding, N., Ardrón, J., Muñoz, P., et al. (2018). A multi criteria assessment method for identifying Vulnerable Marine Ecosystems in the North-East Atlantic. *Front. Mar. Sci.* 5:460. doi: 10.3389/fmars.2018.00460
- Prieto, E., Gonzalez-Pola, C., Lavin, A., and Holliday, N. (2015). Interannual variability of the northwestern Iberia deep ocean: response to large-scale North Atlantic forcing. *J. Geophys. Res. Oceans* 120, 832–847. doi: 10.1002/2014JC010436
- Roberts, J., Davies, A., Henry, L., Dodds, L., Duineveld, G., Lavaleye, M., et al. (2009). Mingulay reef complex: an interdisciplinary study of cold-water coral habitat, hydrography and biodiversity. *Mar. Ecol. Prog. Ser.* 397, 139–151. doi: 10.3354/meps08112
- Ruprich-Robert, Y., Msadek, R., Castruccio, F., Yeager, S., Delworth, T., and Danabasoglu, G. (2017). Assessing the climate impacts of the observed Atlantic multidecadal variability using the GFDL CM2.1 and NCAR CESM1 global coupled models. *J. Clim.* 30, 2785–2810. doi: 10.1175/JCLI-D-16-0217.1
- Sarafanov, A. (2009). On the effect of the North Atlantic Oscillation on temperature and salinity of the subpolar North Atlantic intermediate and deep waters. *ICES J. Mar. Sci.* 66, 1448–1454. doi: 10.1093/icesjms/fsp094
- Skagseth, Ø., Orvik, K., and Furevik, T. (2004). Coherent variability of the Norwegian Atlantic Slope Current derived from TOPEX/ERS altimeter data. *Geophys. Res. Lett.* 31:L14304. doi: 10.1029/2004GL020057
- Sweetman, A., Thurber, A., Smith, C., Levin, L., Mora, C., Wei, C., et al. (2017). Major impacts of climate change on deep-sea benthic ecosystems. *Elementa Sci. Anthropocene* 5, 4. doi: 10.1525/elementa.203
- Terray, P., Delecluse, P., Labattu, S., and Terray, L. (2003). Sea surface temperature associations with the late Indian summer monsoon. *Clim. Dyn.* 21, 593–618. doi: 10.1007/s00382-003-0354-0
- Thierry, V., de Boissésion, E., and Mercier, H. (2008). Interannual variability of the subpolar mode water properties over the Reykjanes Ridge during 1990–2006. *J. Geophys. Res.* 113:C04016. doi: 10.1029/2007JC004443
- Tulloch, R., and Marshall, J. (2012). Exploring mechanisms of variability and predictability of Atlantic meridional overturning circulation in two coupled climate models. *J. Clim.* 25, 4047–4080. doi: 10.1175/JCLI-D-11-00460.1
- Visbeck, M., Chassignet, E., Curry, R., Delworth, T., Dickson, R., and Krahnmann, G. (2013). “The ocean’s response to North Atlantic Oscillation variability,” in *The North Atlantic Oscillation: Climatic Significance and Environmental Impact*, eds J. Hurrell, Y. Kushnir, G. Ottersen, and M. Visbeck, (Washington, DC: American Geophysical Union).
- Yang, Q., Dixon, T., Myers, P., Bonin, J., Chambers, D., van den Broeke, M., et al. (2016). Recent increases in Arctic freshwater flux affects Labrador Sea convection and Atlantic overturning circulation. *Nat. Commun.* 7:10525. doi: 10.1038/ncomms10525
- Yashayaev, I. (2007). Hydrographic changes in the Labrador Sea, 1960–2005. *Prog. Oceanogr.* 73, 242–276. doi: 10.1016/j.pocean.2007.04.015
- Yashayaev, I., Bersch, M., and Van Aken, H. (2007a). Spreading of the Labrador Sea water to the Irminger and Iceland Basins. *Geophys. Res. Lett.* 34:L10602. doi: 10.1029/2006GL028999
- Yashayaev, I., and Seidov, D. (2015). The role of the Atlantic water in multidecadal variability in the Nordic and Barents Seas. *Prog. Oceanogr.* 132, 68–127. doi: 10.1016/j.pocean.2014.11.009
- Yashayaev, I., van Aken, H. M., Holliday, N. P., and Bersch, M. (2007b). Transformation of the Labrador Sea water in the subpolar North Atlantic. *Geophys. Res. Lett.* 34:L22605. doi: 10.1029/2007GL031812
- Yeager, S. (2015). Topographic coupling of the Atlantic overturning and Gyre circulations. *J. Phys. Oceanogr.* 45, 1258–1284. doi: 10.1175/JPO-D-14-0100.1
- Zhang, R. (2008). Coherent surface-subsurface fingerprint of the Atlantic meridional overturning circulation. *Geophys. Res. Lett.* 35:L20705. doi: 10.1029/2008GL035463
- Zunino, P., Lherminier, P., Mercier, H., Daniault, N., Garcia-Ibanez, M., and Perez, F. (2017). The GEOVIDE cruise in May–June 2014 reveals an intense Meridional overturning circulation over a cold and fresh subpolar North Atlantic. *Biogeosciences* 14, 5323–5342. doi: 10.5194/bg-14-5323-2017

Conflict of Interest: The authors declare that the research was conducted in the absence of any commercial or financial relationships that could be construed as a potential conflict of interest.

Copyright © 2020 Johnson, Inall, Gary and Cunningham. This is an open-access article distributed under the terms of the Creative Commons Attribution License (CC BY). The use, distribution or reproduction in other forums is permitted, provided the original author(s) and the copyright owner(s) are credited and that the original publication in this journal is cited, in accordance with accepted academic practice. No use, distribution or reproduction is permitted which does not comply with these terms.